AD-A124 272 DYNAMIC BEHAVIOR OF PARTICULATE VISCOELASTIC COMPOSITES 1/1
FOR SOUND ABSORPT..(U) NAVAL SURFACE WEAPONS CENTER
SILVER SPRING MD G GAUNAURD ET AL. 18 OCT 82
UNCLASSIFIED NSWC/TR-82-520 SBI-AD-F500 117 F/G 20/1 NL

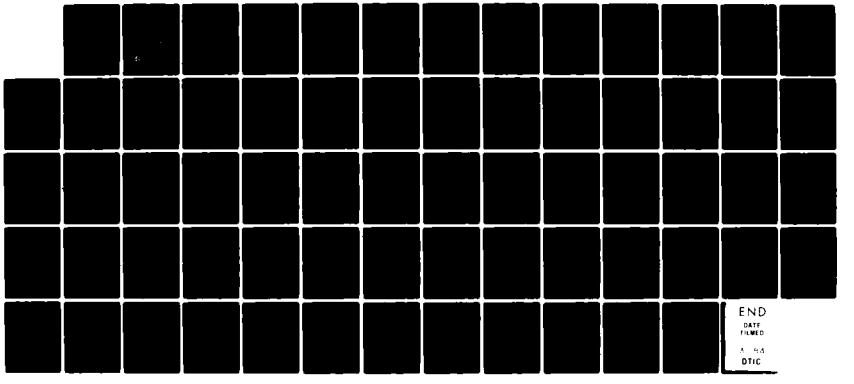

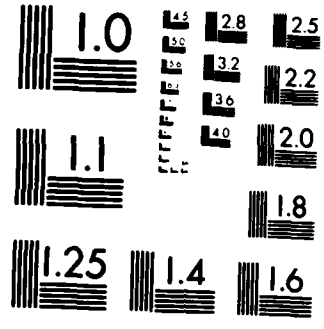

F500 117

12

NSWC TR 82-520

AD A124272

DYNAMIC BEHAVIOR OF PARTICULATE VISCOELASTIC COMPOSITES FOR SOUND ABSORPTION

BY G. C. GAUNAURD J. BARLOW

RESEARCH AND TECHNOLOGY DEPARTMENT

1 OCTOBER 1982

Approved for public release, distribution unlimited

NAVAL SURFACE WEAPONS CENTER

Dahlgren, Virginia 22448 • Silver Spring, Maryland 20910

UNCLASSIFIED

SECURITY CLASSIFICATION OF THIS PAGE (When Data Entered)

REPORT DOCUMENTATION PAGE		READ INSTRUCTIONS BEFORE COMPLETING FORM
1. REPORT NUMBER NSWC TR 82-520	2. GOVT ACCESSION NO. AD-A124 972	3. RECIPIENT'S CATALOG NUMBER
4. TITLE (and Subtitle) DYNAMIC BEHAVIOR OF PARTICULATE VISCOELASTIC COMPOSITES FOR SOUND ABSORPTION		5. TYPE OF REPORT & PERIOD COVERED 6. PERFORMING ORG. REPORT NUMBER
7. AUTHOR(s) G. Gaunaurd and J. Barlow		8. CONTRACT OR GRANT NUMBER(s) N0002482WR10067AD
9. PERFORMING ORGANIZATION NAME AND ADDRESS Naval Surface Weapons Center (Code R43) White Oak Silver Spring, MD 20910		10. PROGRAM ELEMENT, PROJECT, TASK AREA & WORK UNIT NUMBERS 62633N/SF33326602
11. CONTROLLING OFFICE NAME AND ADDRESS Naval Ocean Systems Center (Code 6351) San Diego, CA 92132		12. REPORT DATE 18 October 1982 13. NUMBER OF PAGES 67
14. MONITORING AGENCY NAME & ADDRESS(if different from Controlling Office) Naval Ocean Systems Center (Code 6351) San Diego, CA 92132 and Naval Surface Weapons Center (Code R04) White Oak, Silver Spring, MD 20910		15. SECURITY CLASS. (of this report) UNCLASSIFIED 15a. DECLASSIFICATION/DOWNGRADING SCHEDULE

16. DISTRIBUTION STATEMENT (of this Report)

Approved for public release; distribution unlimited.

17. DISTRIBUTION STATEMENT (of the abstract entered in Block 20, if different from Report)

18. SUPPLEMENTARY NOTES

Excerpts presented at a meeting of the Acoustical Society of America and to be published in their journal.

19. KEY WORDS (Continue on reverse side if necessary and identify by block number)

Sound Absorption	Rubber-like Materials
Particulate Composites	Effective Properties
Viscoelasticity	Frequency-dependent (i.e., Dynamic) Behavior

20. ABSTRACT (Continue on reverse side if necessary and identify by block number)

We have developed a general frequency-dependent theory for the effective material properties (i.e., sound speed, attenuation, bulk, dilatational and shear moduli, etc.) of viscoelastic (i.e., sound absorbing) substances which contain ensembles of gas-filled cavities--assumed spherical for this analysis--of various concentrations and size distributions. The method accounts for the frequency dependence of the effective properties in a fundamental way based on the first principles of Mechanics, that permits the

DD FORM 1 JAN 73 1473 EDITION OF 1 NOV 65 IS OBSOLETE
S/N 0102-LF-014-6601

UNCLASSIFIED

SECURITY CLASSIFICATION OF THIS PAGE (When Data Entered)

study of resonance effects present in all the spectra of all the effective properties we have determined. Our method accounts for the presence of many cavities of various sizes, all embedded within the matrix. It also accounts for the primary interactions of the incident wave with all the cavities, although for the concentration levels considered here, re-scattering and multiple interaction between the various cavities have an effect of secondary magnitude and thus, they have been neglected. Our method acco-nts for the presence of any arbitrary level of dilatational and/or shear viscous absorption in the matrix (the fluid inclusions are assumed lossless) in a fundamental way emerging from basic viscoelastic continuum models such as Kelvin-Voigt's.

Many numerical results were computed and displayed in the spectral plots for air-filled cavities in lossy rubbers that we produced. These cases have included cavity radii in the range $0.0002\ \text{cm} \leqslant a \leqslant 0.125\ \text{cm}$, and various concentration levels below 25%. In all instances the plots exhibit the dominance of the giant monopole resonance. We showed how our present analysis contains nearly all (mostly static) effective properties results available in the literature (including Chaban's), and we included a critical study of the region of validity of the assumptions behind our present approach. We identified four instances where the present method requires additional corrections and we discussed applications of this model to some specific underwater absorber designs. We generated computer codes to calculate all the predictions in all instances. Numerous calculations have been generated at various absorption levels and for cases where the cavities are either all of the same uniform size or when they follow some simple size distribution function.

FOREWORD

The study reported here introduces a novel methodology to predict the (frequency-dependent) effective material parameters characterizing the dynamic behavior of viscoelastic substances containing many randomly located air-filled perforations. These composite materials have uses as underwater sound-absorbers. The methodology described here is an extension of earlier work of the authors which pertains to the case of gas-filled perforations in non-absorbing matrices. That prior work was extended here to the case of absorbing matrices containing ensembles of cavities of various sizes following arbitrary size-distribution functions. The method accounts for the effect of resonances, for arbitrary levels of viscosity, for arbitrary cavity-size distributions, and it is fundamental insorfar as it generates direct predictions accounting for all these effects starting straight from the basic principles of Continuum Mechanics. Computer codes to implement the model-predictions were generated, and a large number of pertinent plots of the frequency dependence (at fixed concentrations) or of the concentration dependence (at fixed frequencies) of the various effective moduli and other material descriptors have been computed and displayed in 88 graphs. Under various conditions the present results reduce to many of the earlier results available in the literature which serve as check points. We have identified four relevant situations where additional work is required to develop corrections to this general approach.

The authors gratefully acknowledge the support and encouragement received by the Naval Ocean Systems Center, San Diego, CA, particularly Mr. S. Speidel, Mr. R. Bologna and Mr. J. Campbell. Part of this work was additionally supported by NSWC Independent Research Board, D. J. Pastine, Director.

Approved by:

Ira M Blatstein

IRA M. BLATSTEIN, Head
Radiation Division

CONTENTS

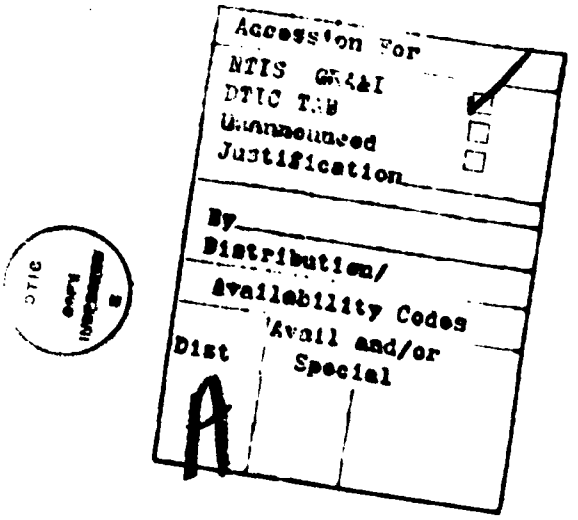

ILLUSTRATIONS

INTRODUCTION

We have developed a general theory to model and predict the effective dynamic material properties (i.e., moduli, wavespeeds, attenuations, densities,...) describing the behavior of elastic matrices containing random distributions of fluid-filled spherical cavities.[1] We have taken that theory,[1] which accounts for resonances and frequency-dependent effects, and extended it here to the case of lossy or sound-absorbing viscoelastic matrices containing the same types of distributions of fluid-filled cavities. The methodology followed to generate this extension is based on scattering theory, and is the same we used to treat the case of purely elastic matrices. The Kelvin-Voigt viscoelastic model was used to describe the rubber behavior in the manner we have explained earlier.[2] A summary of the basic results is given below.

[1] G. Gaunaurd and H. Überall, "Resonance Theory of the Effective Properties of Perforated Solids," J. of the Acoustical Soc. America, Vol. 71, No. 2, 1982, pp. 282-295.

[2] G. Gaunaurd, "Methods For Solving the Viscoelastic Equations For Cylinder and Sphere Problems," NSWC TR-76-20, 22 Mar 1976, 28 pp., (ADA025302).

I. THEORETICAL PREDICTIONS FOR LOSSY MATRICES

The effective properties are determined by this model by relations of the type

$$\phi(\vec{r},\vec{r}_o) = \sum_{j=1}^{N} \phi^{(j)}(\vec{r},\vec{r}_j) \tag{1}$$

which were derived in ref. 1 (i.e., Eq. (3)).

The scattering coefficients pertinent to the analysis to be developed here are A_o, A_1 and A_2. Coefficient A_o takes the form

$$A_o = \frac{x_{d_1}^3}{3i}\left[\frac{3 - x_{of}^2 - x_{os}^2 + x_{oi}^2}{x_{d_1}^2(1 + ix_{d_1}) - x_{of}^2 - x_{os}^2 + x_{oi}^2}\right] \tag{2}$$

where x_{of}, x_{os} and x_{oi}, now for lossy matrices are,

$$x_{of}^2 = \frac{3\rho_2}{\rho_1} \cdot \frac{c_{d_2}^2}{c_{d_1}^2} \cdot \frac{1}{1 - 2i\beta_{d_1}} \tag{3a}$$

$$x_{os}^2 = \left(\frac{2c_{s_1}}{c_{d_1}}\right)^2 \cdot \frac{1 - i2\beta_{s_1}}{1 - i2\beta_{d_1}} \tag{36}$$

$$x_{oi}^2 = \frac{\rho_2}{\rho_1}\left(\frac{2c_{s_2}}{c_{d_1}}\right)^2 \cdot \frac{1}{1 - i2\beta_{d_1}} \quad .$$

We assume that the matrix is lossy, while the fluid inclusions (medium 2) are not.

The definitions of β_{d_1}, β_{s_1} which we have given before,[3] can now be used to express the wave numbers in the viscoelastic matrix as follows.

$$\kappa_{d_1} = \frac{\omega}{c_{d_1}\sqrt{1 - i2\beta_{d_1}}} = \frac{2\pi f}{c_{d_1}}\sqrt{\frac{1}{2} \cdot \frac{\sqrt{1 + 4\beta_{d_1}^2} + 1}{1 + 4\beta_{d_1}^2}} + i\,\frac{2\pi f}{c_{d_1}}\sqrt{\frac{1}{2} \cdot \frac{\sqrt{1 + 4\beta_{d_1}^2} - 1}{1 + 4\beta_{d_1}^2}} \tag{4a}$$

$$\kappa_{s_1} = \frac{\omega}{c_{s_1}\sqrt{1 - i2\beta_{s_1}}} = \frac{2\pi f}{c_{s_1}}\sqrt{\frac{1}{2} \cdot \frac{\sqrt{1 + 4\beta_{s_1}^2} + 1}{1 + 4\beta_{s_1}^2}} + i\,\frac{2\pi f}{c_{s_1}}\sqrt{\frac{1}{2} \cdot \frac{\sqrt{1 + 4\beta_{s_1}^2} - 1}{1 + 4\beta_{s_1}^2}} \quad . \tag{4b}$$

In the absence of losses, these wavenumbers reduce to the known expressions ω/c_{d_1} and ω/c_{s_1}, respectively. Substituting A_o into the corresponding relation

$$\tilde{A}_o(R) = \sum_{j=1}^{N} A_o(a_j) \tag{5}$$

[3] G. Gaunaurd and H. Überall, "Theory of Resonant Scattering From Spherical Cavities in Elastic and Viscoelastic Media," J. Acoustical Society of America, Vol. 63, 1978, pp. 1699-1712.

yields the following expression:

$$\frac{1 - \left[\frac{\rho_1 c_{d_1}^2}{\tilde{\rho}_2 \tilde{c}_{d_2}^2}(1 - 2i\beta_{d_1}) - \frac{4}{3}\frac{\rho_1 c_{s_1}^2}{\tilde{\rho}_2 \tilde{c}_{d_2}^2}(1 - 2i\beta_{s_1})\right] - \frac{4}{3}\frac{\tilde{\rho}_2 \tilde{c}_{s_2}^2}{\tilde{\rho}_2 \tilde{c}_{d_2}^2}}{1 + \frac{4}{3}\frac{\tilde{\rho}_1 \tilde{c}_{s_1}^2}{\rho_2 c_{d_2}^2}(1 - 2i\beta_{s_1}) - \frac{4}{3}\frac{\tilde{\rho}_2 \tilde{c}_{s_2}^2}{\tilde{\rho}_2 \tilde{c}_{d_2}^2}} = \Psi \qquad (6)$$

where

$$\Psi \equiv \sum_{j=1}^{N} \frac{a_j^3}{R^3} \cdot \frac{1 - \left[\frac{\rho_1 c_{d_1}^2}{\rho_2 c_{d_2}^2}(1 - 2i\beta_{d_1}) - \frac{4}{3}\frac{\rho_1 c_{s_1}^2}{\rho_1 c_{d_2}^2}(1 - 2i\beta_{s_1})\right]}{1 - \frac{1}{3}\frac{\rho_1 c_{d_1}^2}{\rho_2 c_{d_2}^2}(1 - 2i\beta_{d_1})x_{d_j}^2(1 + ix_{d_j}) + \frac{4}{3}\frac{\rho_1 c_{s_1}^2}{\rho_2 c_{d_2}^2}(1 - 2i\beta_{s_1})} \qquad (7)$$

defines the parameter Ψ and $x_{d_j} \equiv \kappa_{d_1} a_j$. Manipulating this expression in the manner outlined before [1] we eventually find

$$\Psi = \frac{4\pi}{3} \int_0^\infty \frac{G + iH}{P(a,f) + iQ(a,f)} a^3 g(a) da \qquad (8)$$

where

$$G = 1 - \frac{\rho_1 c_{d_1}^2}{\rho_2 c_{d_2}^2} + \frac{4}{3}\frac{\rho_1 c_{s_1}^2}{\rho_2 c_{d_2}^2},$$

$$H = \frac{\rho_1 c_{d_1}^2}{\rho_2 c_{d_2}^2} \cdot 2\beta_{d_1} - \frac{4}{3}\frac{\rho_1 c_{d_1}^2}{\rho_2 c_{d_2}^2} \cdot 2\beta_{s_1}, \qquad (9a)$$

$$P(a,f) = 1 + \frac{4}{3}\frac{\rho_1 c_{s_1}^2}{\rho_2 c_{d_2}^2} - \frac{1}{3}\frac{\rho_1 c_{d_1}^2}{\rho_2 c_{d_2}^2}\left(\frac{2\pi fa}{c_{d_1}}\right)^2 +$$

$$+ \frac{1}{3}\frac{\rho_1 c_{d_1}^2}{\rho_2 c_{d_2}^2}\left(\frac{2\pi fa}{c_{d_1}}\right)^3 \sqrt{\frac{1}{2}\cdot\frac{\sqrt{1+4\beta_{d_1}^2}-1}{1+4\beta_{d_1}^2}}\ ,$$

$$Q(a,f) = -\frac{1}{3}\frac{\rho_1 c_{d_1}^2}{\rho_2 c_{d_2}^2}\left(\frac{2\pi af}{c_{d_1}}\right)^3 \sqrt{\frac{1}{2}\cdot\frac{\sqrt{1+4\beta_{d_1}^2}+1}{1+4\beta_{d_1}^2}} - \frac{4}{3}\frac{\rho_1 c_{s_1}^2}{\rho_2 c_{d_2}^2}(2\beta_{s_1}) \qquad (9b)$$

and g(a) is the presumably known distribution of cavity sizes. The real and imaginary parts of Ψ are defined as

$$\Psi_R(f) \equiv \frac{4\pi}{3}\int_o^\infty \frac{GP(a,f) + HQ(a,f)}{[P(a,f)]^2 + [Q(a,f)]^2}\, a^3 g(a)da, \qquad (10a)$$

$$\Psi_I(f) \equiv \frac{4\pi}{3}\int_o^\infty \frac{HP(a,f) - GQ(a,f)}{[P(a,f)]^2 + [Q(a,f)]^2}\, a^3 g(a)da, \qquad (10b)$$

where G, H, P, and Q are as before and where

$$\Psi = \Psi_R + i\,\Psi_I\ . \qquad (11)$$

We note that Ψ (c/o Eq. (7)) is frequency-dependent. If it were not (i.e., if $x_{dj} \equiv 0$), then the ratio multiplying (a_j^3/R^3) in Eq. (7), would not depend on j and could come out of the sum. In this static case, Ψ would just be <u>proportional</u> to the concentration Φ, defined to be

$$\Phi = \frac{1}{R^3}\sum_{j=1}^{N} a_j^3\ . \qquad (12)$$

In the dynamic case analyzed here, this is <u>not</u> the case and the concentration is defined to be

$$\Phi = \frac{4\pi}{3} \int_o^\infty g(a) a^3 da \ . \tag{13}$$

If all the cavities are of the same size a_o, then all the a_j will be a_o and then

$$g(a) \equiv \frac{N}{\frac{4\pi}{3}R^3} \delta(a - a_o),$$

and either Eq. (12) or (13) will yield $\Phi \equiv Na_o^3/R^3$. In this uniform cavity-size distribution case we have:

$$\Psi = \left(\frac{G + iH}{P + iQ}\right) \Phi \tag{14}$$

and

$$\Psi_R(f) = \frac{(GP + HQ)\Phi}{[P(a_o,f)]^2 + [Q(a_o,f)]^2} \tag{15a}$$

$$\Psi_I(f) = \frac{(HP - GQ)\Phi}{[P(a_o,f)]^2 + [Q(a_o,f)]^2} \ . \tag{15b}$$

So, we will use either Eqs. (10) or Eqs. (15) depending on whether there is a non-uniform distribution of cavity sizes or all the cavities are of the same sizes, respectively.

The effective bulk modulus $\tilde{k}_{e_2}$ is now given by the (normalized) expression

$$\frac{\tilde{k}_{e_2}}{\rho_1 c_{d_1}^2} = \frac{1 - 2i\beta_{d_1}}{1 - \Psi} - \frac{4}{3} \frac{\rho_1 c_{s_1}^2}{\rho_1 c_{d_1}^2} (1 - 2i\beta_{s_1}) \ , \tag{16}$$

which can be re-written in the following form

$$\frac{\tilde{k}_{e_2}}{\rho_1 c_{d_1}^2} = \frac{\hat{U} + i\hat{V}}{X + iY} = \frac{X\hat{U} + Y\hat{V}}{X^2 + Y^2} + i\left(\frac{X\hat{V} - Y\hat{U}}{X^2 + Y^2}\right) \ , \tag{17}$$

where the parameters X, Y, $\hat{U}$ and $\hat{V}$ are given by

$$X = 1 - \Psi_R(f) \quad , \qquad Y = -\Psi_I(f) \tag{18}$$

$$\hat{U} = 1 - \frac{4}{3}\frac{\rho_1 c_{s_1}^2}{\rho_1 c_{d_1}^2}\left[(1 - \Psi_R) - 2\beta_{s_1}\Psi_I\right] \quad , \tag{19}$$

$$\hat{V} = \frac{4}{3}\frac{\rho_1 c_{s_1}^2}{\rho_1 c_{d_1}^2}\left[\Psi_I + 2\beta_{s_I}(1 - \Psi_R)\right] - 2\beta_{d_1} \quad , \tag{20}$$

and Ψ_R, Ψ_I are given by either Eqs. (10) or (15). Another alternative form still, is,

(21)

$$\frac{\tilde{k}_{e_2}}{\rho_1 c_{d_1}^2} = \left[\frac{(1 - \Psi_R) + 2\beta_{d_1}\Psi_I}{(1 - \Psi_R)^2 + \Psi_I^2} - \frac{4}{3}\frac{\rho_1 c_{s_1}^2}{\rho_1 c_{d_1}^2}\right] + i\left[\frac{\Psi_I - \beta_{d_1}(1 - \Psi_R)}{(1 - \Psi_R)^2 + \Psi_I^2} + \frac{8}{3}\beta_{s_1}\frac{\rho_1 c_{s_1}^2}{\rho_1 c_{d_1}^2}\right]$$

The expressions for the effective shear modulus and the effective shear speed emerge from coefficient A_2. We had already found it[1] for <u>elastic</u> matrices to be

$$A_2 = -\frac{4x_{d_1}^2}{3i} \cdot \frac{\rho_1 c_{s_1}^2(\mu_2 - \rho_1 c_{s_1}^2)}{\mu_2(6\rho_1 c_{d_1}^2 + 4\rho_1 c_{s_1}^2) + \rho_1 c_{s_1}^2(9\rho_1 c_{d_1}^2 - 4\rho_1 c_{s_1}^2)} \quad . \tag{22}$$

For a viscoelastic matrix with fluid inclusions we find, in an analogous way,

$$A_2 = -\frac{4x_{d_1}^3}{3i}\frac{\rho_1 c_{s_1}^2(1 - 2i\beta_{s_1})\left[\mu_2 - \rho_1 c_{s_1}^2(1 - 2i\beta_{s_1})\right]}{R + S} \tag{23}$$

where

$$R = \mu_2\left[6\rho_1 c_{d_1}^2(1 - i2\beta_{d_1}) + 4\rho_1 c_{s_1}^2(1 - 2i\beta_{s_1})\right] \tag{24a}$$

$$S = \rho_1 c_{s_1}^2(1 - 2i\beta_{s_1})\left[9\rho_1 c_{d_1}^2(1 - 2i\beta_{d_1}) - 4\rho_1 c_{s_1}^2(1 - 2i\beta_{s_1})\right] \quad . \tag{24b}$$

Substituting Eq. (23) into the basic "effective property" relation for A_2,

$$\tilde{A}_2(R) = \sum_{j=1}^{N} A_2(a_j) \tag{25}$$

eventually yields the effective (normalized) shear modulus

$$\frac{\tilde{\mu}_2}{\mu_1} = \frac{M + iN}{K + iL} + \frac{MK + NL}{K^2 + L^2} + i \left(\frac{NK - ML}{K^2 + L^2} \right) , \tag{26}$$

where M, N, K and L are

$$M = \left[(9\rho_1 c_{d_1}^2 - 4\rho_1 c_{s_1}^2) + 2\beta_{s_1} (8\rho_1 c_{s_1}^2 \beta_{s_1} - 18\rho_1 c_{d_1}^2 \beta_{d_1}) \right] (1 - \Phi)$$

$$N = \left[(8\rho_1 c_{s_1}^2 \beta_{s_1} - 18\rho_1 c_{d_1}^2 \beta_{d_1}) - 2\beta_{s_1} (9\rho_1 c_{d_1}^2 - 4\rho_1 c_{s_1}^2) \right] (1 - \Phi)$$

$$K = (9\rho_1 c_{d_1}^2 - 4\rho_1 c_{s_1}^2) + (6\rho_1 c_{d_1}^2 + 4\rho_1 c_{s_1}^2)\Phi$$

$$L = (8\rho_1 c_{s_1}^2 \beta_{s_1} - 18\rho_1 c_{d_1}^2 \beta_{d_1}) - 2\beta_{s_1} (9\rho_1 c_{d_1}^2 - 4\rho_1 c_{s_1}^2)\Phi \quad . \tag{27}$$

Once the effective bulk modulus and the effective shear modulus are known, we can construct the effective dilatational (or compressional) modulus by the relation,

$$\tilde{M}_{d_2} \equiv \tilde{\rho}_2 \tilde{c}_{d_2}^2 = \tilde{k}_{e_2} + \frac{4}{3}\tilde{\mu}_2 . \tag{28}$$

Substituting Eqs. (26) and (17) into (28) eventually yields,

$$\frac{\tilde{\rho}_2 \tilde{c}_{d_2}^2}{\rho_1 c_{d_1}^2} = \frac{U + iV}{X + iY} = \frac{XU + YV}{X^2 + Y^2} + i \left(\frac{XV - YU}{X^2 + Y^2} \right) \tag{29}$$

where U and V (without carets) are now

$$U = 1 - \frac{4}{3}\frac{\rho_1 c_{s_1}^2}{\rho_1 c_{d_1}^2}\left[\left(1 - \frac{MK + NL}{K^2 + L^2}\right)(1 - \Psi_R) - \left(2\beta_{s_1} + \frac{NK - ML}{K^2 + L^2}\right)\Psi_I\right] \quad (30a)$$

$$V = \frac{4}{3}\frac{\rho_1 c_{s_1}^2}{\rho_1 c_{d_1}^2}\left[\left(1 - \frac{MK + NL}{K^2 + L^2}\right)(\Psi_I) + \left(2\beta_{s_1} + \frac{NK - ML}{K^2 + L^2}\right)(1 - \Psi_R)\right] - 2\beta_{d_1}, \quad (30b)$$

where X, Y, M, N, K and L are as above. An alternative form for this (normalized) effective dilatational modulus is,

$$\frac{\tilde{\rho}_2 \tilde{c}_{d_2}^2}{\rho_1 c_{d_1}^2} = \left[\frac{1 - \Psi_R + 2\Psi_I \beta_{d_1}}{(1 - \Psi_R)^2 + \Psi_I^2} - \frac{4}{3}\frac{\rho_1 c_{s_1}^2}{\rho_1 c_{d_1}^2}\left(1 - \frac{MK + NL}{K^2 + L^2}\right)\right] +$$

$$+ i\left[\frac{\Psi_I - 2\beta_{d_1}(1 - \Psi_R)}{(1 - \Psi_R)^2 + \Psi_I^2} + \frac{4}{3}\frac{\rho_1 c_{s_1}^2}{\rho_1 c_{d_1}^2}\left(2\beta_{s_1} + \frac{NK - ML}{K^2 + L^2}\right)\right] . \quad (31)$$

These expressions for the effective dilatational modulus $\tilde{\rho}_2 \tilde{c}_{d_2}^2$ can be solved for the effective dilatational wavespeed $\tilde{c}_{d_2}$. The effective wavenumber $\tilde{\kappa}_{d_2}$ is

$$\tilde{\kappa}_{d_2} = \mathrm{Re}\left(\frac{\omega}{\tilde{c}_{d_2}}\right) + i\,\mathrm{Im}\left(\frac{\omega}{\tilde{c}_{d_2}}\right) \equiv \frac{\omega}{\tilde{c}_2} + i\,\tilde{\alpha}_2 \quad (32)$$

and it is therefore possible to relate the (real) effective sound speed $\tilde{c}_2$ and the real attenuation $\tilde{\alpha}_2$, to the (complex) effective dilatational speed $\tilde{c}_{d_2}$, just determined, by the following relations:

$$\frac{\tilde{c}_2}{c_{d_1}} = \frac{1}{\sqrt{1 - (1 - \rho_2/\rho_1)\Phi}} \sqrt{\frac{2(U^2 + V^2)}{\sqrt{X^2 + Y^2}\sqrt{U^2 + V^2} + XU + YV}} = \frac{\omega / c_{d_1}}{\mathrm{Re}\left(\frac{\omega}{\tilde{c}_{d_2}}\right)} \qquad (33)$$

$$\tilde{\alpha}_2 a_o = -\frac{2\pi f a_o}{c_{d_1}} \operatorname{sign}\left[\Psi_I\right] \sqrt{1 - (1 - \rho_2/\rho_1)\Phi}$$

$$\cdot \sqrt{\frac{\sqrt{X^2 + Y^2}\sqrt{U^2 + V^2} - (XU + YV)}{2(U^2 + V^2)}} = a_o \, \mathrm{Im}\,(\omega/\tilde{c}_{d_2}). \qquad (34)$$

These are the same expressions we found for elastic matrices,[1] the difference being the new definitions of X, Y, U, V, Ψ_R and Ψ_I for the lossy matrix case.

The effective density emerges out of coefficient A_1 and it happens to be the same as for elastic matrices, viz.,

$$\tilde{\rho}_2 = (1 - \Phi)\,\rho_1 + \rho_2 \Phi \quad . \qquad (35)$$

The effective shear speed can now be given for viscoelastic matrices in the form

$$\tilde{c}_{s_2} = \sqrt{\frac{\tilde{\mu}_2}{\tilde{\rho}_2}} = \sqrt{\frac{\mu_1}{\rho_1\left[1 - (1 - \rho_2/\rho_1)\Phi\right]}} \cdot \sqrt{\left(\frac{MK + NL}{K^2 + L^2}\right) + i\left(\frac{NK - ML}{K^2 + L^2}\right)} \qquad (36)$$

where M, N, K, and L are given above. We now give, mainly for completeness since it is never used, the (complex) effective dilatational wavespeed $\tilde{c}_{d_2}$ mentioned above, viz.,

$$\tilde{c}_{d_2} = \frac{c_{d_1}}{\sqrt{1 - (1 - \rho_2/\rho_1)\Phi}} \cdot \sqrt{\frac{U + iV}{X + iY}} \quad , \qquad (37)$$

where X, Y, U and V are all given above. We note that all formulas given here reduce properly to those given in Ref. 1 for fluid-fillers inside the cavities contained within elastic matrices. Furthermore, if the matrix is made to be a fluid matrix (i.e., gas bubbles in a liquid), then all the results here and in Ref. 1 reduce properly to our earlier results for bubbly liquids.[4] This completes this summary of theoretical predictions for absorbing matrices.

The effective Lamé parameter $\tilde{\lambda}_2$ can be computed from the effective bulk $\tilde{k}_{e_2}$, dilatational $\tilde{M}_{d_2} \equiv \tilde{\lambda}_2 + 2\tilde{\mu}_2$, and shear $\tilde{\mu}_2$ moduli by the relations

$$\tilde{\lambda}_2 = \tilde{k}_{e_2} - \frac{2}{3}\tilde{\mu}_2 = \tilde{M}_{d_2} - 2\tilde{\mu}_2.$$

[4]G. Gaunaurd and H. Überall, "Resonance Theory of Bubbly Liquids," J. of the Acoustical Soc. America, Vol. 69, 1981, pp. 362-370.

II. NUMERICAL RESULTS

We will concentrate on air-filled (spherical) cavities in a viscoelastic (rubber) matrix. We first will consider the rubber and the air material parameters as we have given them in our previous Ref. (1). The rubber density is $\rho_1 = 1.13$ g/cm^3, and that of air is $\rho_2 = 0.0012$ g/cm^3. The other parameters are given in Section III of Ref. (1).

For the viscous properties of the rubber we will set β_{s_1} fixed at 5% and consider two values of β_{d_1}, viz., 1% and 5%. These quantities controlling the absorptive parts of κ_{d_1} and κ_{s_1} (see Eqs. (4)) were defined in our Ref. (3). In our earlier notation,[3] to have $\beta_{s_1} = 5\%$ means that $F_1 = 10^7$. To have $\beta_{d_1} = 1\%$ or 5% means that $F = 4.276 \times 10^8$, or $F = 2.218 \times 10^9$, respectively. These numbers were arbitrarily chosen to introduce some level of viscosity in the rubber, and to see how the non-absorbing results plotted in Ref. (1) were altered by the presence of matrix viscosity. However, these values ($\beta_{d_1} \sim 5\%$, $\beta_{s_1} \sim 5\%$) are not uncommon in practice. We have chosen concentrations of $\Phi = 5$ and 10% because these were the numbers selected in Ref. (1), and it was of interest to see how the "effective properties" at these concentrations were altered from the values in Ref. (1), to the present values in the presence of matrix losses. We have stated in earlier work of ours that the present theory neglects re-scattering (i.e., multiple scattering) from the many cavities in the matrix. This assumption ceases to hold for concentrations above 25%, which is the upper limit of validity of this theory, without additional multiple-scattering corrections. In the first few plots that follow, the cavities are of uniform sizes as we will describe next.

Figure 1 shows the real and imaginary parts of the (normalized) effective dilatational modulus $\tilde{M}_{d_2}$ versus frequency for clouds of cavities of 2μm in radius at 5% and 10% concentrations when the matrix has a viscous level of $\beta_{d_1} = 5\%$, and $\beta_{s_1} = 5\%$. The formula plotted is Eq. (29). For the materials and concentrations considered, these plots are undistinguishable from the corresponding plots for the effective bulk modulus $\tilde{k}_{e_2}$ as given by Eq. (17).

Figure 2 shows the same quantities at the same concentrations and viscous levels but for clouds of larger cavities all at uniform 20 micron sizes. The resonance effects are quite visible and are clearly shifted to the lower frequency region. The formulas plotted are Eqs. (29) and/or (17), which yield undistinguishable results for the present materials. At the high frequency ends of the real plots (left) we see that $\tilde{M}_{d_2} \to M_{d_1}$, which means that the effective properties coincide with those of the matrix at high-frequencies and low

concentrations. The numbers in the abscisas are frequencies in megahertz.

The results in Figs. 1 and 2 are to be compared to those in ref. (1), which were computed for the same parameters but without absorption in the matrix (i.e., $\beta_{d_1} = 0$, $\beta_{s_1} = 0$). Viscosity shifts the location of the (giant monopole) resonance to lower frequencies and knocks down its amplitude in the real plots. In the imaginary plots, the amplitude of the dip is less pronounced the higher the viscosity, and the location of the dip is also shifted to the low frequency end. Viscosity also broadens all these resonance peaks (or dips) so that the widths are all increased with absorption, as it should be.

Figures 3 and 4 are companion figures to each other and they display the (normalized) effective sound speed and attenuation for a cloud of air-filled cavities in lossy rubber at $\Phi = 5\%$ (upper graphs) and 10% concentration (lower graphs). All the cavities are of the same uniform size, $a_o = 2$ microns. Figure 3 is for a viscous level (i.e., $\beta_{d_1} = 1\%$, $\beta_{s_1} = 5\%$) and Fig. 4 is for a higher level (i.e., $\beta_{d_1} = 5\%$, $\beta_{s_1} = 5\%$). Both these figures can be compared to analogous ones we have published elsewhere[1] for totally non-absorbing matrices (i.e., $\beta_{d_1} = \beta_{s_1} = 0$). Higher absorptions shift the resonances toward the lower frequency end of the spectrum and broaden the peaks. We have examined these effects in the past[6] in analogous instances for a single cavity. These effects continue to be present for clouds of cavities as we can see. The formulas being plotted in Figs. 3 and 4 are given in Eqs. (33) and (34). High and low frequency limits could be easily found from those expressions, but these will not be investigated analytically here. Numerical values are observable in the plots for these limits.

Figures 5 and 6 are companion figures to each other and they display the (normalized) effective sound speed and attenuation versus frequency for a cloud of air-filled cavities in lossy rubber now all of larger but uniform sizes ($a = 20$ microns). The upper graphs are for $\Phi = 5\%$ and the lower ones for $\Phi = 10\%$. Fig. 5 is for a level of viscosity (i.e., $\beta_{d_1} = 1\%$, $\beta_{s_1} = 5\%$) and Fig. 6 is for a higher level (i.e., $\beta_{d_1} = 5\% = \beta_{s_1}$). Both these figures can be compared to similar ones for no viscosity at all in the matrix which were published elsewhere.[1,5] The pair of Figs. 3 and 4 are analogous to the pair formed by Figs. 5 and 6, the difference being that the first pair corresponds to cavities 2μm in size while the second is for 20 micron cavities.

We recall that the effect of the giant monopole resonance for a single gas-filled cavity in rubber[7] manifests itself at $k_{d_1} a_o \simeq 0.1$, where $k_{d_1} = 2\pi f / c_{d_1}$. For rubber of $c_{d_1} = 1.4 \times 10^5$ cm/sec, that condition translates to

$$f a_o = 2.5 \qquad (38)$$

---

[5] G. Gaunaurd and H. Überall, "Errata: Resonance Theory of the Effective Properties of Perforated Solids," J. of the Acoustical Soc. America (to be published), 1983.

[6] G. Gaunaurd, et al., "New Method To Determine Shear Absorption Using the Visco-elastodynamic Resonance Scattering Formalism," J. of the Acoustical Soc. America, Vol. 64, 1978, pp. 1211-1212.

[7] G. Gaunaurd, et al., "Giant Monopole Resonances in the Scattering of Waves From Gas-filled Spherical Cavities and Bubbles," J. of the Acoustical Soc. America, Vol. 65, 1979, pp. 573-594.

where a_o is in centimeters and f is in kilohertz. When there are many cavities in the rubber, the number on the right side of Eq. (38) is a bit higher (c/o Figs. 3-6) but we will use Eq. (38) for the argument that follows. If we have f = 20 kHz, the first resonance occurs for cavities of size a_o = 0.125 cm. If f = 60 kHz, then the required cavity size for resonance is a_o = 0.0417 cm. So, cavity sizes required for resonance in this frequency range go from 0.4 mm to 1.2 mm.

The effective shear modulus is displayed versus concentration Φ ($0 \leq \Phi \leq 50\%$) at three levels of viscosity in Fig. 7. These graphs exhibit the real and the imaginary parts of the normalized modulus, all computed for air-filled cavities in rubber. The equation being plotted is Eq. (26). For the three absorption levels shown in Fig. 7, the real parts of the modulus exhibit very small changes while the changes in the imaginary parts are more perceptible.

Figure 8 shows the real and imaginary parts of the (normalized) effective shear speed versus concentration Φ for two levels of viscosity (i.e., β_{d_1} = 1%, β_{s_1} = 5% and $\beta_{d_1} = \beta_{s_1}$ = 5% as they are obtained from Eq. (36). Higher absorptions reduce the shear speed in the perforated solid and also its corresponding imaginary part.

A relation for the effective density such as Eq. (35) was plotted, in normalized form in earlier work of ours (viz., ref. (1), Fig. 6) and will not be repeated here.

The computer programs developed to generate Figs. 1-8 could also be used to plot any of the formulas in Section I, for any material combination, absorption levels, concentrations, or distributions of cavity sizes and frequency ranges. Appendix 1 shows the complete listings for these programs.

These programs have been used to compute Figs. 9-12. Figure 9 shows the real (left) and imaginary (right) parts of the (normalized) effective bulk modulus versus frequency for a uniform distribution of cavity sizes all of radius a_o = 0.125 cm at Φ = 10%. The upper plots are for a viscous level of $\beta_{d_1} = \beta_{s_1}$ = 5% while the lower plots are for non-viscous matrices ($\beta_{d_1} = \beta_{s_1}$ = 0%) in order to show the effect of (light) matrix absorption. As in previous figures, these results are numerically equal to those of the (normalized) effective dilatational modulus. The pertinent equations plotted are Eqs. (17) or (29). The frequency ranges are now restricted to the band $0 \leq f \leq 40$ kHz.

Figure 9 shows the effective (and normalized) sound speed and attenuation versus frequency plots for clouds of cavities of (uniform) size a_o = 0.125 cm at Φ = 10%. The upper plots are to be compared ot the lower plots, to see the effect of viscosity. The upper graphs are for the viscous level $\beta_{d_1} = \beta_{s_1}$ = 5%, while the lower ones are for non-lossy matrices (i.e., $\beta_{d_1} = \beta_{s_1}$ = 0%) and are shown for comparison. Resonance effects are clearly observable around 20-24 kHz as one would expect from Eq. (38) for this size cavities, which are the ones resonating for incident waveforms of frequencies 20 kHz. Observation of these plots show that viscosity in the matrix broadens the resonance peaks and shifts them to higher frequencies. A more detailed analysis of this effect could be done with results such as these. The formulas plotted in Fig. 10 are Eqs. (33) and (34).

Figures 11 and 12 are the identical counterparts of Figs. 9 and 10, respectively, but for clouds of cavities of size a_o = 0.0417 cm. These are the sizes that excite the giant monopole resonance (at around 70 kHz) whenever the incident wave is of frequency f = 60 kHz (c/0 Eq. (38)). The frequency range in these figures now includes the broader band $0 \leqslant f \leqslant 100$ kHz. The broadening and shift of the attenuation (i.e., $\tilde{\alpha}_2$) peak with increased absorption is clearly visible in Fig. 12. All plots presented in Figs. 1-12 are for clouds of air-filled cavities in rubber having uniform sizes. In these cases, Ψ_R and Ψ_I are always found from Eqs. (15).

It is of interest to see how these quantities Ψ_R and Ψ_I, as computed from Eqs. (15), behave as functions of frequency. Figure 13 displays these quantities in the range $0 \leqslant f \leqslant 40$ kHz for swarms of air-filled cavities of uniform size a_o = 0.125 cm, and a Φ = 10% concentration. The upper graphs are for no matrix viscosity, while the lower ones are for a moderate matrix viscosity of $\beta_{d_1} = \beta_{s_1}$ = 5%. It is quite clear that viscosity shifts and broadens the resonance peaks.

The rest of the figures (i.e., Figs. 14-22) are all for the case where the cavity sizes are <u>not</u> uniformly distributed. The methodology presented here can analyze and account for arbitrary size distributions g(a). We have selected a triangular distribution of cavity sizes to illustrate this effect in a simple case, although real cavity size-distributions are more likely to be Gaussian, provided the cavities are really randomly located, as opposed to periodically located in a lattice. Figure 14 shows the distribution function and the cummulative distribution function of the triangular distribution. The peak of the distribution is set to occur at value a_o. It can be easily verified that the mean of the triangular distribution is 1.5 times the mean of the uniform distribution function.

Figure 15 shows the same quantities plotted in Fig. 13 (viz., Ψ_R and Ψ_I) in the absence (top) and presence (bottom) of viscosity in the matrix, at a 10% concentration level. The cavities are now triangularly distributed with the peak of the triangular distribution a_o at 0.125 cm. Comparison of Figs. 13 and 15 shows that for triangularly distributed cavities, the resonance peaks are shifted to lower frequencies and broadened to wider widths. The magnitude of the peaks is also reduced. So, cavity size-distributions other than uniform have an effect similar to that of viscosity in the matrix, viz., they lower and broaden the resonances, and knock down their respective amplitudes. Figure 16 is identical to Fig. 15 except that it has now been recomputed for the higher concentration level of Φ = 15%. These observations all emerge from quick inspections of Figs. 13 and 15, and they could be quanitatively analyzed in further detail. Figure 16 shows that a higher concentration of triangularly distributed cavities further <u>increases</u> the size of the peaks, all other things being equal.

Figure 17 is the counterpart of Fig. 9 for triangularly distributed swarms of air-filled cavities in a rubber matrix at 10% concentrations. Now a_o = 0.125 cm is the peak of the triangular distribution. The upper graphs are for moderate matrix viscosity (i.e., $\beta_{d_1} = \beta_{s_1}$ = 5%) while the lower ones are for no viscosity at all. This Fig. 17 displays the real and the imaginary parts of the effective bulk modulus, versus frequency in the range $0 \leqslant f \leqslant 40$ kHz. The graphs in Fig. 17 are very close to those in Fig. 9, except in the middle portion ($f \sim 16$ kHz) where an additional dip is observable. These are the regions where Ψ_R and Ψ_I showed a difference (Fig. 15) in relation to their values for uniform cavity-size distributions (c/o Fig. 13)

Figure 18 is the counterpart of Fig. 10, now for triangularly distributed clouds of cavities at 10% concentrations, where a_o = 0.125 cm is the peak of the triangular distribution. Figure 18 displays in this case the effective sound speed $\tilde{c}_2/c_{d_1}$, and effective attenuation $\tilde{\alpha}_2 a_o$ versus frequency plots. Comparison of Figs. 18 and 10 shows that the triangular distribution of cavities has a very marked effect on the attenuations. The effective sound speed also changes--it is lower now at all frequencies--and there is a smoothing effect in the mid-portions of the graphs where the resonances in Ψ_R, Ψ_I changed substantially. The plots are computed at two levels of viscosity (viz., $\beta_{d_1} = \beta_{s_1} = 5\%$, upper graphs, and $\beta_{d_1} = \beta_{s_1} = 0\%$, lower graphs) as before.

The results in Fig. 17 have been re-computed in Fig. 19 for a 15% concentration, all else being the same. Higher concentrations tend to flatten these spectra, and we indeed see that at low frequencies the real and imaginary parts of the effective bulk moduli in Fig. 19, computed assuming a triangular cavity-size distribution, are lower than in Fig. 17 where the concentration was only 10%. At the higher frequency end of these spectra, we observe higher values in Fig. 19 than those in the corresponding plots of Fig. 17. Thus, higher concentrations have clearly flattened the earlier results.

Figure 20 is the same as Fig. 18 but re-computed at 15% concentrations. It is clear, from inspection of these figures, that higher concentration levels tend to lower the effective sound speeds at all frequencies and to increase the effective attenuations, particularly at the high frequencies beyond that of the giant monopole resonance ($\sim$20 kHz in this case).

We have recomputed Fig. 19 for smaller cavities, still triangularly distributed, but now with peak at a_o = 0.0417 cm. The result is shown in Fig. 21. This figure shows the real and the imaginary parts of the effective bulk modulus versus frequency ($0 \leqslant f \leqslant 100$ kHz) plots, for ensembles of triangularly distributed cavities in rubber, at 15% concentrations. The upper graphs are for a viscous level $\beta_{d_1} = \beta_{s_1} = 5\%$, while the lower graphs are for $\beta_{d_1} = \beta_{s_1} = 0\%$, (no viscosity). Figure 21 (triangular distribution) can also be compared to Fig. 11 (uniform-size distribution), although the concentrations are not the same. The same general remarks made before still hold in this case.

Figure 22 is the re-computation of Fig. 20 but for smaller a_o. Therefore, Fig. 22 gives the effective sound speed and attenuation versus frequency ($0 \leqslant f \leqslant 100$ kHz) plotts, for ensembles of gas-filled cavities in a rubber matrix all triangularly distributed with the peak a_o now at 0.0417 cm. The concentration level is 15% and the same two earlier viscous levels ($\beta_{d_1} = \beta_{s_1} = 5\%$ and $\beta_{d_1} = \beta_{s_1} = 0\%$) are considered. Figure 22 can also be compared to Fig. 12 although the concentrations are slightly different (i.e., 10% versus 15%). Again, the triangular distribution lowers the effective sound speed, particularly at high frequencies, and increases the effective attenuation over a wider frequency band, mainly because of the similar flattening and broadening effects non-uniform distributions and higher viscosity levels have on the resonance peaks. All these effects are quantitatively exhibited in these 22 figures which contain 88 graphs, all computer generated, from the basic theory presented here.

III. DISCUSSION OF THE CHABAN RESULTS

The Chaban results are valid for non-absorptive matrices and they are frequency-independent (i.e., they are static results). Their derivation is based in the so-called self-consistent approach which has been the subject of much controversy and doubt.

For non-absorptive rubber matrices (i.e., $\beta_{d_1} = 0$, $\beta_{s_1} = 0$) containing clouds of uniform size air-filled cavities of radii a_o, the (normalized) effective bulk modulus given in our Eq. (17) reduces to the expressions given in Eqs. (34)-(40) of ref. (1). In the static or long-wavelength limit (i.e., $f \to 0$), that expression contains the well-known Kerner result[8]

$$\tilde{k}_{e_2} = \left[k_{e_1}(1 - \Phi) + k_{e_2}\left(\frac{k_{e_1} + \frac{4}{3}\mu_1}{k_{e_2} + \frac{4}{3}\mu_1}\right)\Phi \right] \Bigg/ \left[1 - \Phi + \left(\frac{k_{e_1} + \frac{4}{3}\mu_1}{k_{e_2} + \frac{4}{3}\mu_1}\right)\Phi \right] \tag{39}$$

which for dilute concentrations ($\Phi << 1$) yields the expression

$$\tilde{k}_{e_2} = k_{e_1} + \left[\left(k_{e_1} + \frac{4}{3}\mu_1\right) \Big/ \left(k_{e_2} + \frac{4}{3}\mu_1\right) \right] \left(k_{e_2} - k_{e_1}\right) \Phi \tag{40}$$

which is Chaban's dilute limit[9] (ref. 9, Eq. (41).

The (normalized) effective shear modulus given in Eq. (26) reduces to the expression in Eq. (45) of our ref. 1 when there are no losses in the rubber matrix ($\beta_{d_1} = \beta_{s_1} = 0$). This later equation, in the dilute limit ($\Phi << 1$) agrees with Chaban's dilute limit formula which is

$$\tilde{\mu}_2 = \mu_1 - \frac{5}{2}\Phi\left(1 - \frac{\mu_2}{\mu_1}\right)(\lambda_1 + 2\mu_1)E, \tag{41}$$

---

[8] E. H. Kerner, "The Elastic and Thermoelastic Properties of Composite Media," Proc. Phys. Soc. (London), Vol. 69B, 1956, pp. 808-813.

[9] I. A. Chaban, Soviet Phys. - Acoustics, Vol. 10, 1965, pp. 298-304, and, Vol. 11, 1965, pp. 81-86.

where E is a parameter defined by

$$E \equiv \frac{6}{2\frac{\mu_2}{\mu_1}\cdot\frac{3\lambda_1 + 8\mu_1}{\mu_1} + \frac{9\lambda_1 + 14\mu_1}{\mu_1}} \quad . \tag{42}$$

It is not hard to show that this expression coincides with the expression we gave in our ref. 1 (Eq. (80)), viz.,

$$\frac{\tilde{\mu}_2}{\mu_1} = 1 - \frac{15(1-\nu_1)\left(1 - \frac{\mu_2}{\mu_1}\right)\Phi}{7 - 5\nu_1 + 2(4 - 5\nu_1)\left(\frac{\mu_2}{\mu_1}\right)} \quad , \tag{43}$$

in terms ofthe Poisson's ratio ν_1 of the matrix. Therefore, our frequency-dependent method presented here for absorbing matrices, greatly extends and contains the static and non-absorbing results of Chaban in the dilute limit.

Finally, for air-filled (or evacuated) cavities in rubber (assumed lossless) Eqs. (39) and (43) yield, approximately,

$$\frac{\tilde{k}_{e_2}}{k_{e_1}} = \frac{(1-\Phi)}{1 + \frac{3}{4}\frac{k_{e_1}}{\mu_1}\Phi} \tag{44}$$

$$\frac{\tilde{\mu}_2}{\mu_1} = 1 - \frac{5}{3}\Phi \tag{45}$$

which are results due to Gassmann and Dewey, respectively, and which we already studied in our earlier work.[1] These static formuli are sometimes quoted by absorber designers.

IV. DISCUSSION OF ASSUMPTIONS AND REGIONS OF VALIDITY OF THE METHODOLOGY

FUTURE PLANS

A variety of assumptions were made during the construction of the methodology described here. Some of the most important ones are as follows: a) The cavities are assumed small compared to the wavelength of the incident wave. In spite of this small a/λ assumption, resonance effects are present, and are taken into account by the method, since the dominant giant monopole resonance occurs at very low a/λ-values. b) The volume concentrations, Φ, of cavities within the matrix are assumed small (i.e., $\Phi < 25\%$). This implies that the possible multiple scattering effects that would be present for densely packed configurations, are of secondary importance and to first orders, may be neglected. c) All the observations are made in the far-field of the effective sphere[1] (i.e., $r >> R$) so that only the global effects of the ensemble of cavities are noticed at the observation point. This condition is met for either low concentrations (i.e., $\Phi << 1$), low frequencies, or small cavity sizes ($a/\lambda << 1$). d) The giant monopole resonance has a dominant effect over all others and manifests itself very strongly at very low a/λ - ratios. We have shown this to be true[7] for air-filled cavities in rubber matrices, weather the rubber is assumed lossy or not. This assumption does not hold true for solid inclusions, and the whole analysis presented here must be modified in that case. e) The cavities are all contained in a boundless matrix of infinite extent (i.e., no boundaries are present). Therefore, the present model works best when the cavities are small compared to the layer thickness. When the incident waveforms are of low frequencies, the cavity sizes required to excite their giant monopole resonance (i.e., the lowest), could be large enough to make them comparable in size to the thickness of the matrix (or layer) that contains them. In this case, an additional correction must be introduced into the analysis to account for the nearby presence of boundaries or layer edges. At higher frequencies of the incident wave, the required cavity sizes became small compared to the matrix thickness, the thickness correction becomes negligible, and the boundless matrix approach presented here remains valid. We have described the case where the cavity size and layer thickness are of comparable sizes, as a "correction" to the boundless matrix approach described here. This is so because the cavity size will still control the location of the resonance, however, the finite layer-thickness will shift it, broaden it, and modify it from its unbounded value. A numerical example will quantitatively illustrate these points.

Assume there is a (thick) rubber layer covering an underwater structure that is 10 cm (4 inches) thick. This is not an unrealistic thickness if the coating is to absorb effectively in the low-end of the frequency spectrum. At frequencies of f = 20 kHz, we can obtain an estimate for the cavity size required to excite the first (i.e., the giant monopole) resonance from Eq. (38). This estimated value is a = 0.125 cm (i.e. one-and-a-quarter millimeter). This size

is about a fiftieth of the layer thickness and hence, the theory developed here applies quite adequately. In fact, for such frequencies, and such (small) cavity sizes, one does not need such a thick layer. In fact, a thickness of about 1 cm will still be adequate to permit the application of the present model without any additional corrections. For incident frequencies of f = 60 kHz, Eq. (38) would yield resonating cavity sizes of value a_o = 0.042 cm, which are even smaller when compared to the layer thickness than before, and thus the layer thickness could be reduced even further to perhaps 1/3 cm. without modifications. If, on the other hand we had lower incident frequencies (say, f ≈ 2.5 kHz), then Eq. (38) would yield cavities of diameter 2 cm, which is still relatively small compared to the 10 cm layer-thickness, provided there is only one such row of cavities within the layer as it is often the case. It is for these "large" cavities which lie close to the layer edges that we should introduce edge-corrections or finite-thickness corrections, not accounted for in the present analysis.

There seems to be no upper limit on the levels of viscosity (compressional or shear) that could be used within this model. Either type of viscosity could well be as high as 100% without any foreseeable complications. We have already seen that for single cavities, higher levels of viscosity produce shifts in the resonance frequencies and broadenings of the resonance peaks.[6] This phenomenon has not been examined in detail within the context of the present model for many cavities within a matrix.

Inequalities of some design importance are $\lambda >> L >> a$, where L is the layer thickness and "a" the cavity radius. A further rule of thumb between layer and cavity dimensions is $L > 6a$.

The model assumes spherical cavities. The shape of the cavities appears to be irrelevant provided that the air contents (i.e, volume) of any two possible shapes, as well as their concentration, remains the same. This follows from conditions a) and b), since we are dealing with small cavities compared to the layer thickness and the wavelength of the incident sound wave. Under the present assumptions a) - e), this model will apply to specific absorber designs such as AA-17 provided one develops the finite-thickness corrections for the layer which is needed under assumption e). We make this statement specifying this correction, even though the frequencies at which AA-17 is most effective are quite high, because the specific design calls for cavities which are very close to the layer edges. At the relatively low (under 25%) cavity concentrations present in AA-17, it seems reasonable to assume that the cylindrical cavities could be replaced by equivalent spherical ones of the same volume and concentration, without introducing much error in the final results. This conjecture should also be further investigated and to this end we have already devised a plan to study the monopole resonance of finite-length cylindrical cavities.

In summary, four further corrections should be included in the analysis for various instances. For densely packed inclusion configurations, additional multiple scattering corrections have to be developed. For the low frequencies requiring the large resonating cavities having walls near to the layer edges, we must introduce corrections to account for the finite layer-thickness. For cavities with shapes other than spherical, particularly at high frequencies, shape corrections should be considered. Of particular interest is the case of finite cylindrical cavities, for which even the giant monopole resonance is not well understood. Fourth, some absorber designs call for the introduction of

solid inclusions in the matrix rather than fluid ones (i.e., gas-filled cavities). This final instance requires further study, for both elastic and viscoelastic matrices. Finally, there seems to be no upper viscosity level beyond which the present model fails. We have developed research plans to thoroughly study and understand all four of these modifications and/or corrections, in future work. The model also takes into account arbitrary cavity size distribution functions. Numerous calculations have been performed and displayed in two basic instances. The first is for the case when all the cavities are of the same uniform size a_o. The second is for the case when some cavities are larger than others, the whole collection following the simple (but arbitrarily chosen) triangular distribution function of peak (mean) value a_o. We have produced many quantitative plots for the variations of the most significant quantities, in both instances. The overall effect of non-uniform (triangular in this case) cavity size distributions is analogous to that of a higher viscous absorption level, viz., it shifts the actual resonance locations, broadens their peaks and smoothes-out or diminishes their spectral amplitudes.

V. SUMMARY AND CONCLUSIONS

In the present work we have developed a general theory to predict the dynamic effective material properties of lossy perforated matrices with fluid-fillers. These composites are considered to be viscoelastic (i.e., sound absorbing) matrices containing random distributions of fluid-filled spherical cavities or perforations of various sizes. The method accounts for the losses in the rubberlike material in a fundamental way which emerges from the basic principles of mechanics and the Kelvin-Voigt viscoelastic model.[2] Hence, the method does not proceed in an ad-hoc way as it has been done by authors who have derived[10] (or repeated the derivations of earlier[11]) lossless theories and "extended them" by assuming complex wavenumbers or complex wavespeeds which can not be related to observed material properties in a systematic (or any other) way.[10] Our method is based on scattering theory[1] and thus, it yields frequency-dependent results in a natural way. This frequency-dependence of results is again found from the fundamental laws of mechanics and it is to be contrasted with other approaches which are static but then they are "made to be frequency-dependent" by introducing experimentally observed data, fitted by approximate means, into the analytic expressions for the static results. Thirdly, our method accounts for the actual presence of many cavities of many sizes within the matrix, the effects of each one added by the technique. This is unlike other approaches that have dealt only with one such cavity in the matrix[12,10] and merely stated that if there had been many, the effects would have been additive under some sort of addition law of effective behavior that (incredibly) was never really produced.[10] Although these authors[10] talk about the effective behavior of the composite, the composite they have considered has only one hole, and matrix viscosity is introduced fictitiously in the ad-hoc fashion we mentioned above.

Our method stays away from the procedures used in the "self-consistent method"[9] because of the conceptual difficulties and the inconsistencies

---

[10] R. L. Kligman, et al., "Effective Dynamic Properties of Composite Viscoelastic Materials," J. of the Acoustical Soc. America, Vol. 70, 1981, pp. 1437-1444.

[11] N. Yamakawa, "Scattering and Attenuation of Elastic Waves, Parts I and II," Geophys. Magaz. (Tokyo), Vol. 31, 1962, pp. 63-103.

[12] E. Meyer, et al., "Pulsation Oscillations of Cavities in Rubber," J. of the Acoustical Soc. America, Vol. 30, 1958, pp. 1116-1124.

associated with that approach,[13] that have seriously questioned its validity. The present analysis yields results that reduce properly to every previously published static result[1] not using the self-consistent method, and also to the few dynamic results that are available for simpler matrix/filler combinations.[4]

The present method yields effective, frequency-dependent, analytic expressions for the effective moduli (bulk, dilatational, and shear), effective density, effective sound speed and effective attenuation, for a viscoelastic (lossy) medium of large extent, containing many fluid-filled spherical cavities of various sizes. All results are checked by showing their proper degeneration into simpler results[1] published earlier.

Numerical results were computed and displayed for air-filled cavities in lossy rubbers for various cases. We initially considered cavity sizes and viscous losses extending the inviscid results of ref. 1. We then used the developed computer codes to make additional runs for cases where resonating cavities around (incident) frequencies of 20 kHz and 60 kHz were of concern. The analysis has demonstrated the dominance of the giant monopole resonance in all the plotted cases, (i.e., sound speed, attenuations, real and imaginary parts of the bulk modulus, etc....). The cavity volume concentrations were varied as well as the amount of viscous loss in the absorbing matrix. Criteria for the estimation of the location of the giant monopole resonance emerged from the study and we observed in the resulting graphs how higher viscous levels shifted the resonance peaks and broadened their widths. Further analytic studies of these effects should be made in the future.

We studied and discussed the static results of Chaban[9] and demonstrated how these emerge as very particular cases of the present results in the absence of viscous losses, for dilute concentrations, and in the long wavelength limit, which are the conditions for the Chaban results to hold true.

We made a critical study of the regions of validity of the series of assumptions behind the present methodology. We found it universally valid under the ordinary procedures used for high-frequency absorber design. We were able to isolate four cases in which additional corrections are required to modify the present results. These cases are: a) densely packed cavities of high volume concentration, b) large resonating cavities comparable in size to the thickness of the layer which contained them, c) shape corrections for other than spherical cavity shapes particularly when the cavities lie near or on the layer edges, and d) inclusions of solid (rather than fluid) composition within a lossless or even a lossy matrix. We have developed a plan of attack to analyze each of these modifications in the future.

This analysis has included a detailed study of the effect of (non-uniform) cavity size distributions on the various effective quantities of interest, which were quantitatively displayed in many graphs (i.e., Figs. 15-22). Non-uniform (triangular in this case, c/o Fig. 14) cavity size distributions tend to have the same smoothing effect on the effective material parameters of the composite

[13] R. M. Christensen, Mechanics of Composite Materials, J. Wiley & Sons, New York, 1979, p. 60.

that seems to be observed at higher viscous levels. They shift the resonances, reduce their amplitudes, and broaden their widths over wider spectral regions. All these considerations and quantitative displays provide the building blocks of the trade off studies that must be conducted by absorber designers in order to understand and construct efficient underwater sound absorbers.

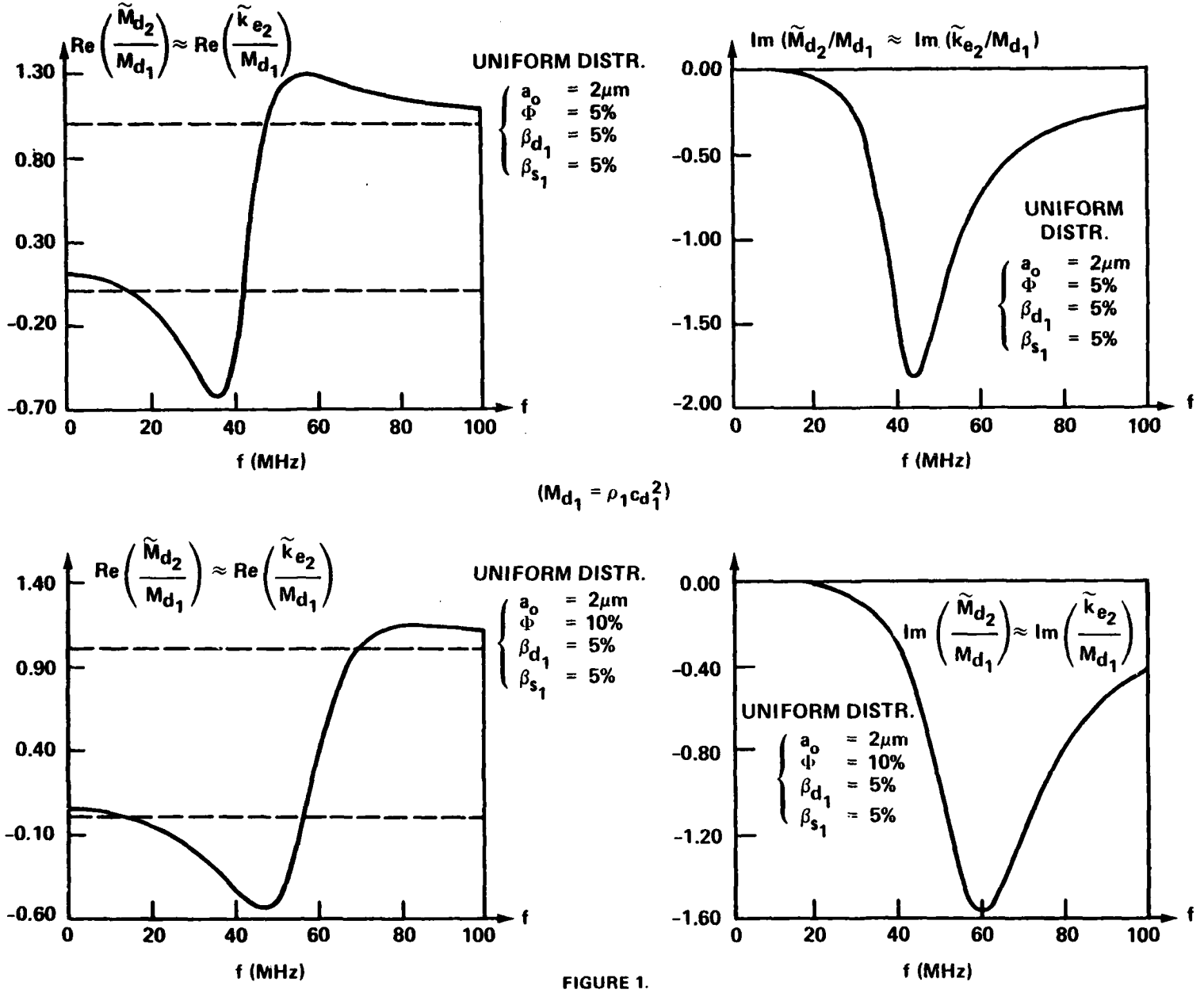
Re $\left(\frac{\tilde{M}_{d_2}}{M_{d_1}}\right) \approx$ Re $\left(\frac{\tilde{k}_{e_2}}{M_{d_1}}\right)$
UNIFORM DISTR.
a_o = 2μm
Φ = 5%
β_{d_1} = 5%
β_{s_1} = 5%
1.30
0.80
0.30
-0.20
-0.70
0 20 40 60 80 100
f (MHz)
f
Im $(\tilde{M}_{d_2}/M_{d_1} \approx$ Im $(\tilde{k}_{e_2}/M_{d_1})$
0.00
-0.50
-1.00
-1.50
-2.00
UNIFORM DISTR.
a_o = 2μm
Φ = 5%
β_{d_1} = 5%
β_{s_1} = 5%
0 20 40 60 80 100
f (MHz)
f
$(M_{d_1} = \rho_1 c_{d_1}^2)$
Re $\left(\frac{\tilde{M}_{d_2}}{M_{d_1}}\right) \approx$ Re $\left(\frac{\tilde{k}_{e_2}}{M_{d_1}}\right)$
UNIFORM DISTR.
a_o = 2μm
Φ = 10%
β_{d_1} = 5%
β_{s_1} = 5%
1.40
0.90
0.40
-0.10
-0.60
0 20 40 60 80 100
f (MHz)
f
Im $\left(\frac{\tilde{M}_{d_2}}{M_{d_1}}\right) \approx$ Im $\left(\frac{\tilde{k}_{e_2}}{M_{d_1}}\right)$
UNIFORM DISTR.
a_o = 2μm
Φ = 10%
β_{d_1} = 5%
β_{s_1} = 5%
0.00
-0.40
-0.80
-1.20
-1.60
0 20 40 60 80 100
f (MHz)
f

FIGURE 1.

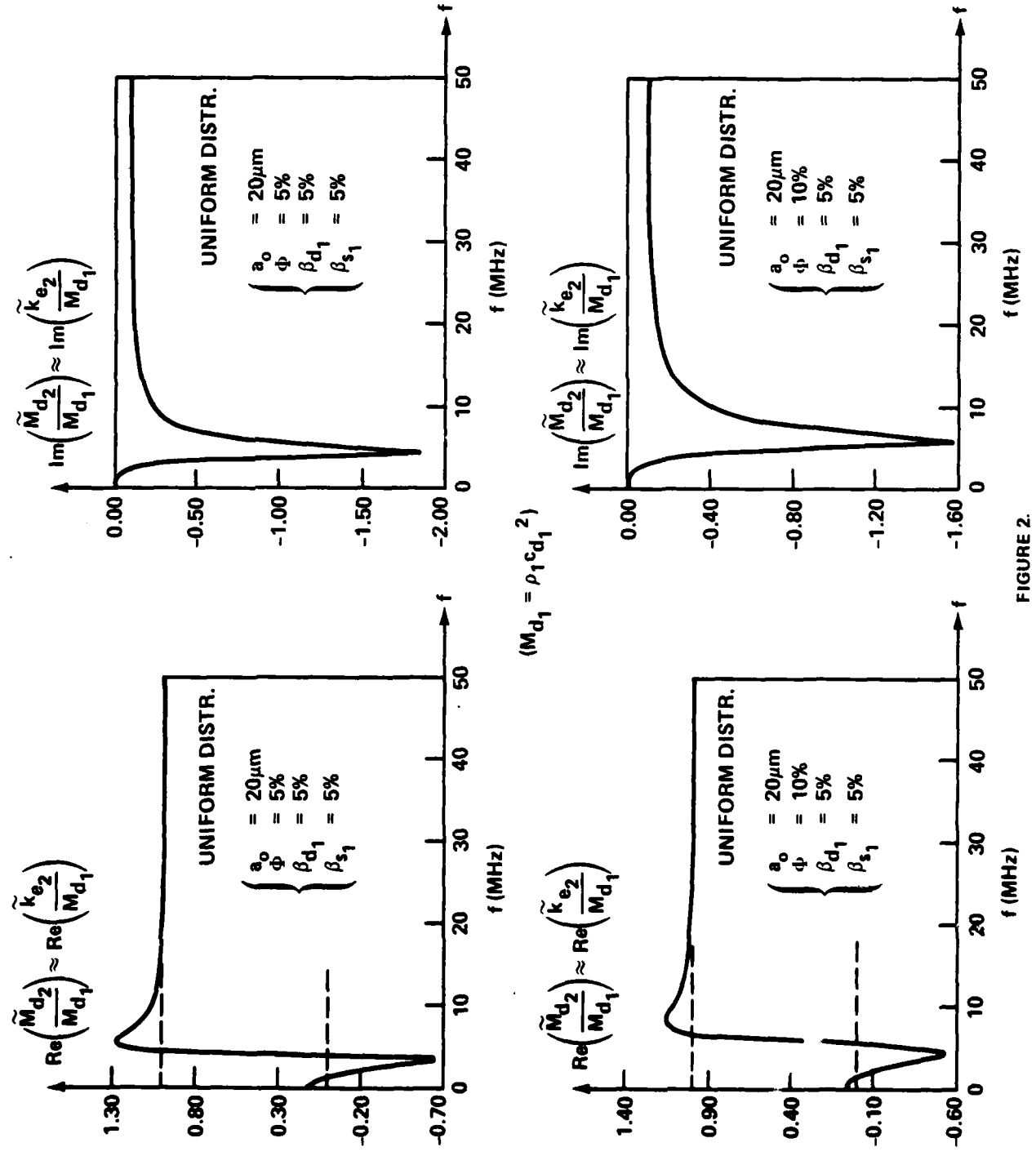
UNIFORM DISTR.
a_o = 20μm
Φ = 5%
β_{d_1} = 5%
β_{s_1} = 5%
$\mathrm{Re}\left(\frac{\tilde{M}_{d_2}}{M_{d_1}}\right) \approx \mathrm{Re}\left(\frac{\tilde{k}_{e_2}}{M_{d_1}}\right)$
$\mathrm{Im}\left(\frac{\tilde{M}_{d_2}}{M_{d_1}}\right) \approx \mathrm{Im}\left(\frac{\tilde{k}_{e_2}}{M_{d_1}}\right)$
f (MHz)
f
$(M_{d_1} = \rho_1 c_{d_1}^2)$

FIGURE 2.

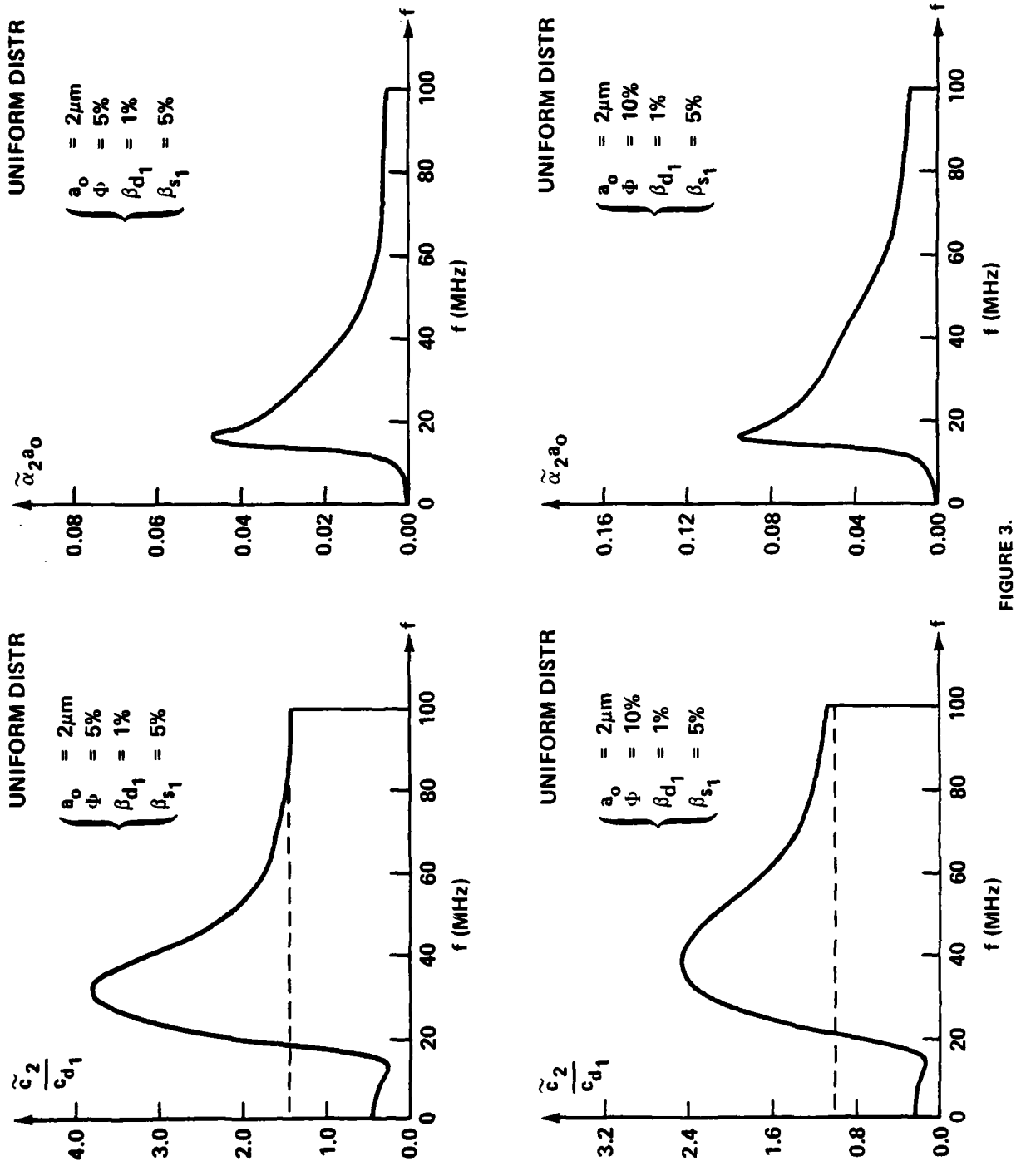
UNIFORM DISTR
a_o = 2μm
Φ = 5%
β_{d_1} = 1%
β_{s_1} = 5%
$\tilde{\alpha}_2 a_o$
0.08
0.06
0.04
0.02
0.00
0
20
40
60
80
100
f
f (MHz)
UNIFORM DISTR
a_o = 2μm
Φ = 10%
β_{d_1} = 1%
β_{s_1} = 5%
$\tilde{\alpha}_2 a_o$
0.16
0.12
0.08
0.04
0.00
0
20
40
60
80
100
f
f (MHz)
UNIFORM DISTR
a_o = 2μm
Φ = 5%
β_{d_1} = 1%
β_{s_1} = 5%
$\frac{\tilde{c}_2}{c_{d_1}}$
4.0
3.0
2.0
1.0
0.0
0
20
40
60
80
100
f
f (MHz)
UNIFORM DISTR
a_o = 2μm
Φ = 10%
β_{d_1} = 1%
β_{s_1} = 5%
$\frac{\tilde{c}_2}{c_{d_1}}$
3.2
2.4
1.6
0.8
0.0
0
20
40
60
80
100
f
f (MHz)

FIGURE 3.

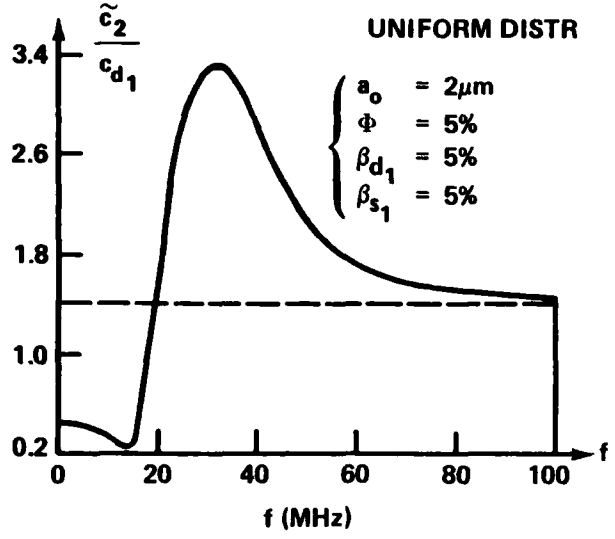
$\frac{\tilde{c}_2}{c_{d_1}}$
UNIFORM DISTR
a_o = 2μm
Φ = 5%
β_{d_1} = 5%
β_{s_1} = 5%
3.4
2.6
1.8
1.0
0.2
0
20
40
60
80
100
f
f (MHz)

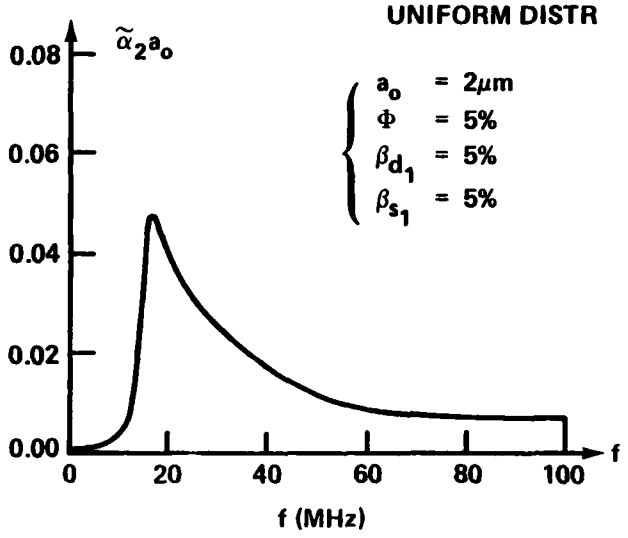
$\tilde{\alpha}_2 a_o$
UNIFORM DISTR
a_o = 2μm
Φ = 5%
β_{d_1} = 5%
β_{s_1} = 5%
0.08
0.06
0.04
0.02
0.00
0
20
40
60
80
100
f
f (MHz)

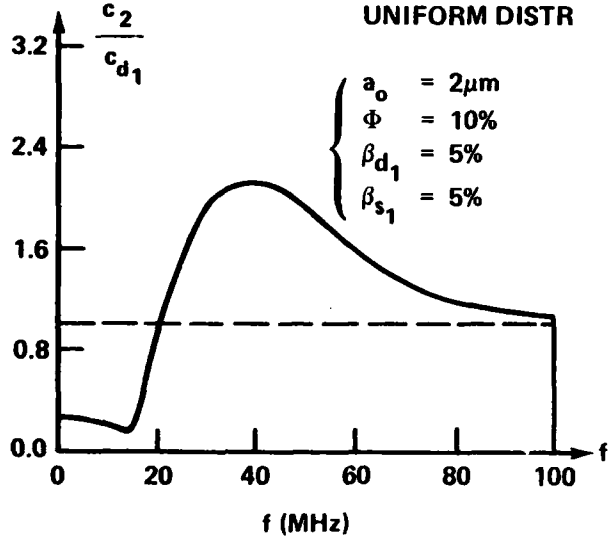
$\frac{\tilde{c}_2}{c_{d_1}}$
UNIFORM DISTR
a_o = 2μm
Φ = 10%
β_{d_1} = 5%
β_{s_1} = 5%
3.2
2.4
1.6
0.8
0.0
0
20
40
60
80
100
f
f (MHz)

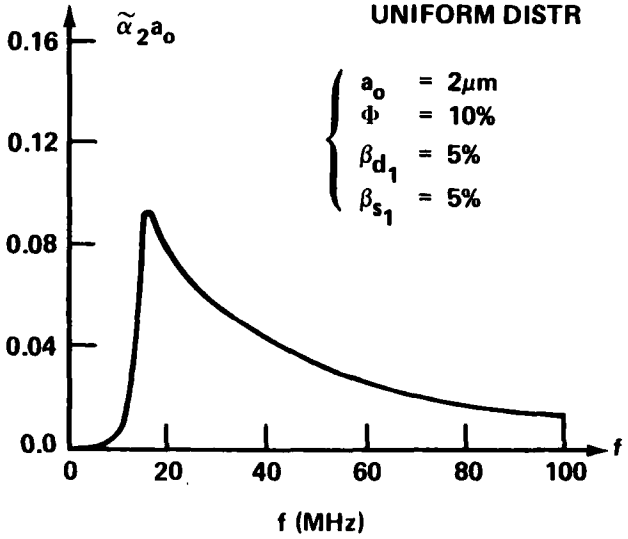
$\tilde{\alpha}_2 a_o$
UNIFORM DISTR
a_o = 2μm
Φ = 10%
β_{d_1} = 5%
β_{s_1} = 5%
0.16
0.12
0.08
0.04
0.0
0
20
40
60
80
100
f
f (MHz)

FIGURE 4.

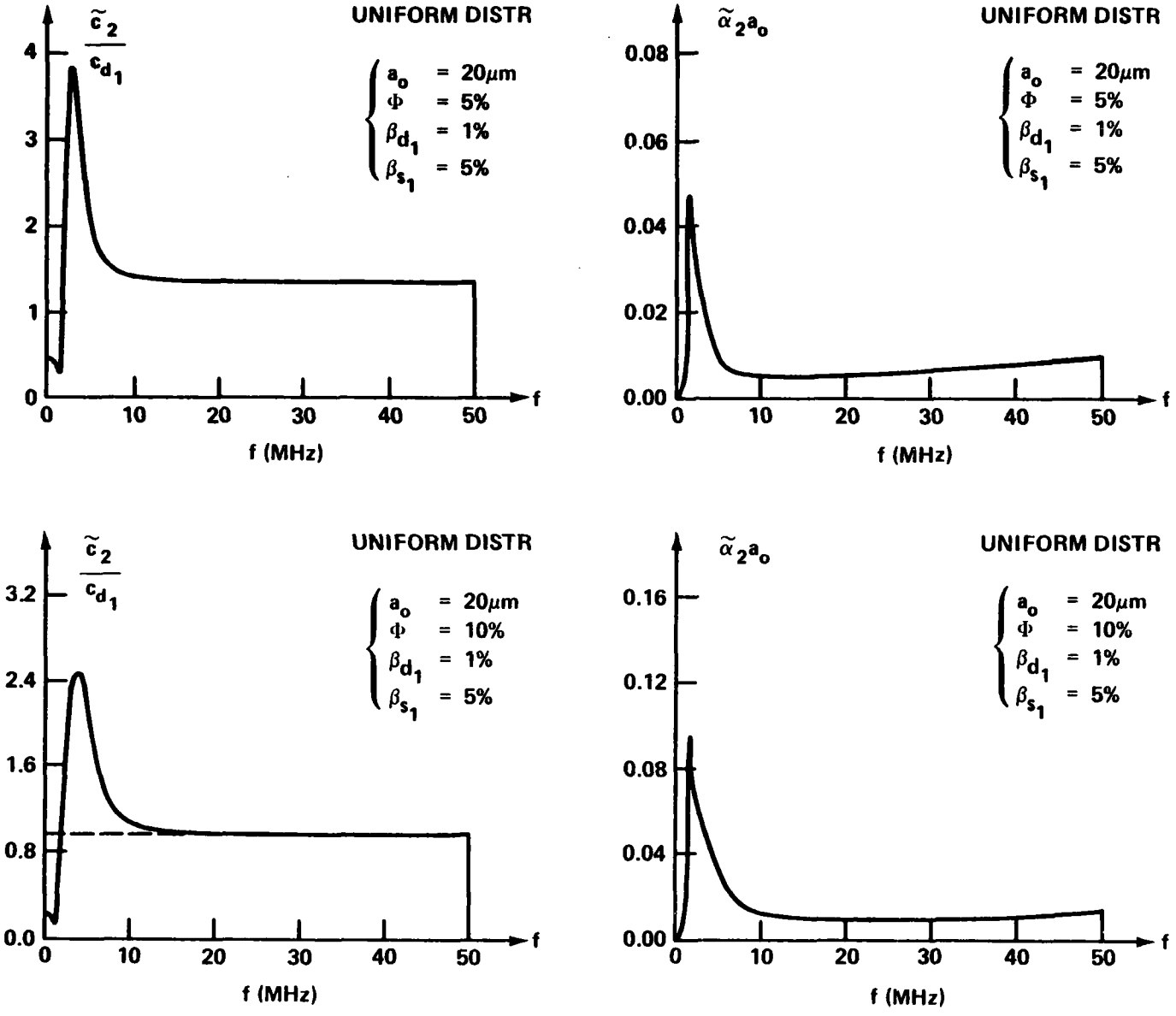
$\tilde{c}_2 / c_{d_1}$
UNIFORM DISTR
a_o = 20μm
Φ = 5%
β_{d_1} = 1%
β_{s_1} = 5%
f (MHz)
$\tilde{\alpha}_2 a_o$
UNIFORM DISTR
a_o = 20μm
Φ = 5%
β_{d_1} = 1%
β_{s_1} = 5%
f (MHz)
$\tilde{c}_2 / c_{d_1}$
UNIFORM DISTR
a_o = 20μm
Φ = 10%
β_{d_1} = 1%
β_{s_1} = 5%
f (MHz)
$\tilde{\alpha}_2 a_o$
UNIFORM DISTR
a_o = 20μm
Φ = 10%
β_{d_1} = 1%
β_{s_1} = 5%
f (MHz)

FIGURE 5.

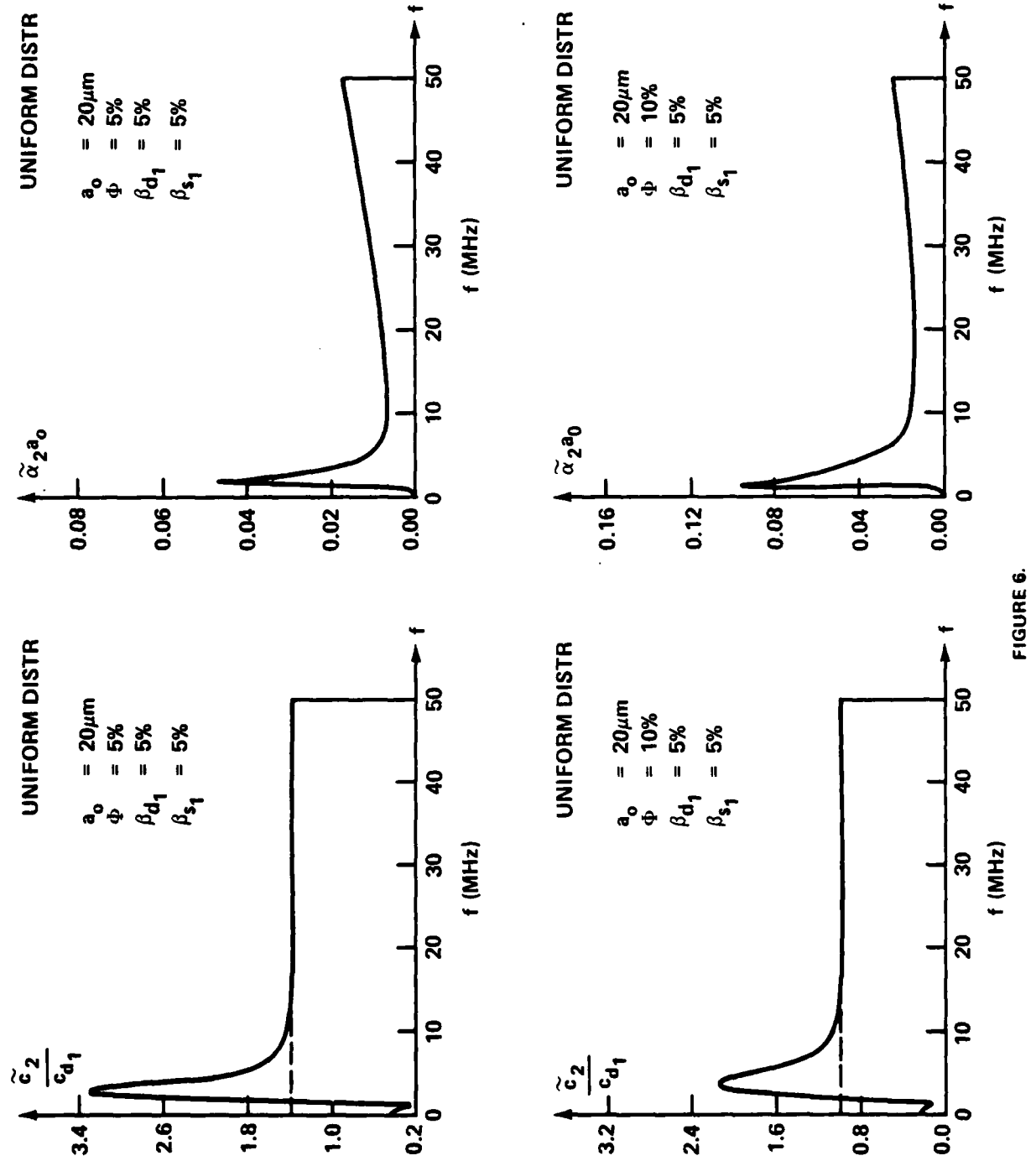
UNIFORM DISTR
a_o = 20μm
Φ = 5%
β_{d_1} = 5%
β_{s_1} = 5%
$\tilde{\alpha}_2 a_o$
0.08
0.06
0.04
0.02
0.00
0
10
20
30
40
50
f
f (MHz)
UNIFORM DISTR
a_o = 20μm
Φ = 10%
β_{d_1} = 5%
β_{s_1} = 5%
$\tilde{\alpha}_2 a_o$
0.16
0.12
0.08
0.04
0.00
0
10
20
30
40
50
f
f (MHz)
UNIFORM DISTR
a_o = 20μm
Φ = 5%
β_{d_1} = 5%
β_{s_1} = 5%
$\frac{\tilde{c}_2}{c_{d_1}}$
3.4
2.6
1.8
1.0
0.2
0
10
20
30
40
50
f
f (MHz)
UNIFORM DISTR
a_o = 20μm
Φ = 10%
β_{d_1} = 5%
β_{s_1} = 5%
$\frac{\tilde{c}_2}{c_{d_1}}$
3.2
2.4
1.6
0.8
0.0
0
10
20
30
40
50
f
f (MHz)

FIGURE 6.

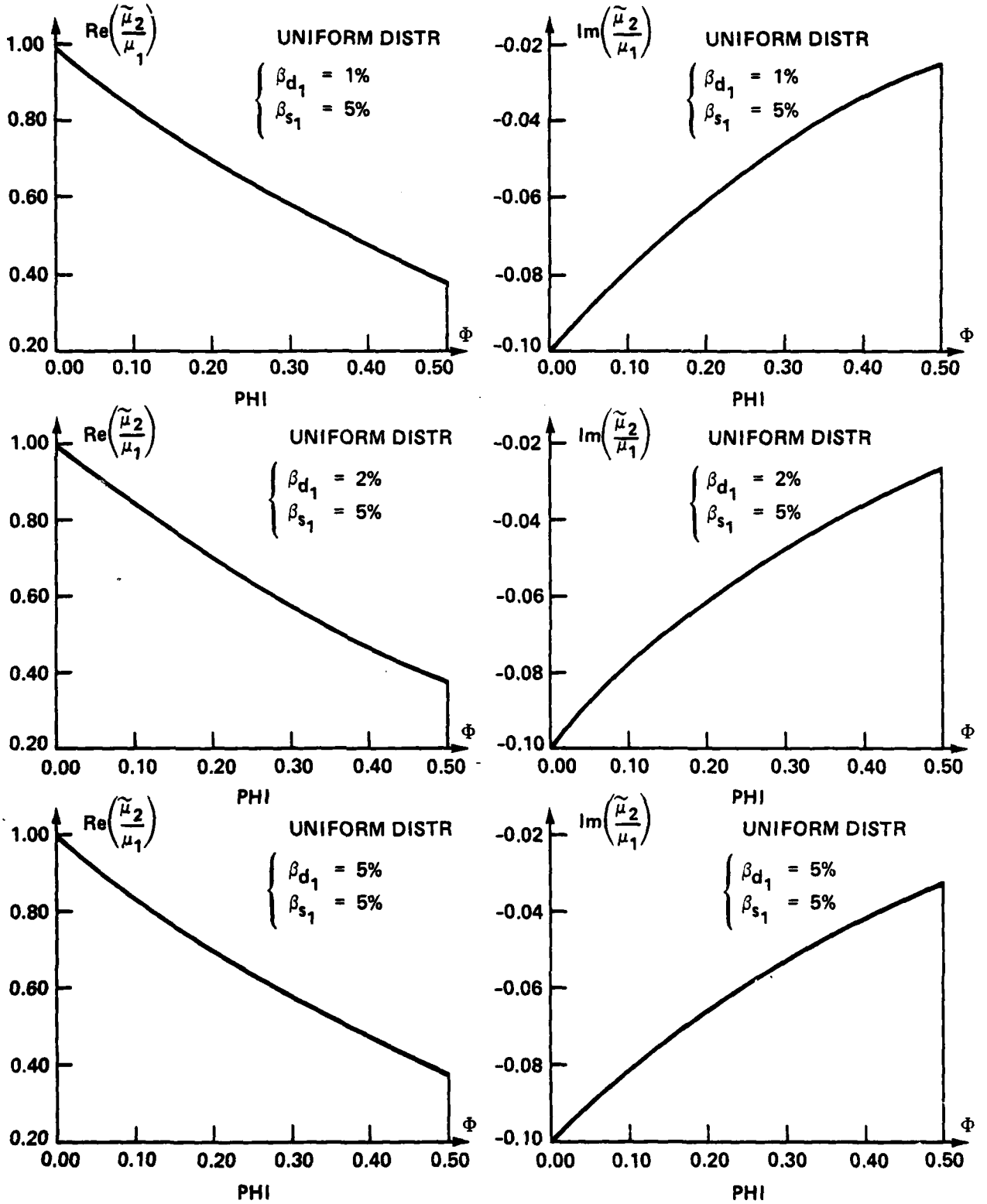
Re($\frac{\tilde{\mu}_2}{\mu_1}$)
UNIFORM DISTR
β_{d_1} = 1%
β_{s_1} = 5%
1.00
0.80
0.60
0.40
0.20
0.00 0.10 0.20 0.30 0.40 0.50
PHI
Φ
Im($\frac{\tilde{\mu}_2}{\mu_1}$)
UNIFORM DISTR
β_{d_1} = 1%
β_{s_1} = 5%
-0.02
-0.04
-0.06
-0.08
-0.10
0.00 0.10 0.20 0.30 0.40 0.50
PHI
Φ
Re($\frac{\tilde{\mu}_2}{\mu_1}$)
UNIFORM DISTR
β_{d_1} = 2%
β_{s_1} = 5%
1.00
0.80
0.60
0.40
0.20
0.00 0.10 0.20 0.30 0.40 0.50
PHI
Φ
Im($\frac{\tilde{\mu}_2}{\mu_1}$)
UNIFORM DISTR
β_{d_1} = 2%
β_{s_1} = 5%
-0.02
-0.04
-0.06
-0.08
-0.10
0.00 0.10 0.20 0.30 0.40 0.50
PHI
Φ
Re($\frac{\tilde{\mu}_2}{\mu_1}$)
UNIFORM DISTR
β_{d_1} = 5%
β_{s_1} = 5%
1.00
0.80
0.60
0.40
0.20
0.00 0.10 0.20 0.30 0.40 0.50
PHI
Φ
Im($\frac{\tilde{\mu}_2}{\mu_1}$)
UNIFORM DISTR
β_{d_1} = 5%
β_{s_1} = 5%
-0.02
-0.04
-0.06
-0.08
-0.10
0.00 0.10 0.20 0.30 0.40 0.50
PHI
Φ

FIGURE 7.

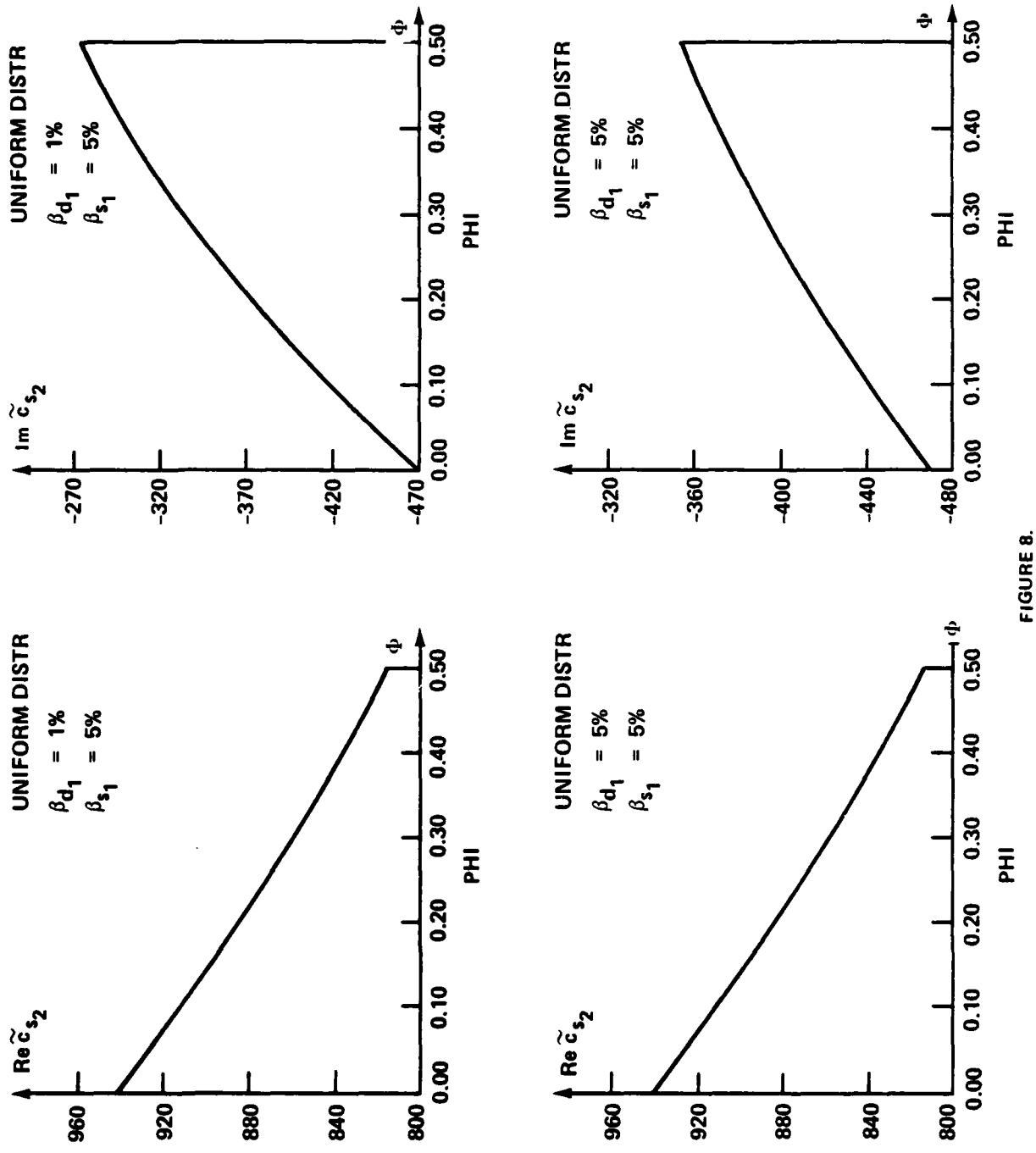
UNIFORM DISTR
β_{d_1} = 1%
β_{s_1} = 5%
Im $\tilde{c}_{s_2}$
-270
-320
-370
-420
-470
0.00
0.10
0.20
0.30
0.40
0.50
PHI
Φ
UNIFORM DISTR
β_{d_1} = 5%
β_{s_1} = 5%
Im $\tilde{c}_{s_2}$
-320
-360
-400
-440
-480
0.00
0.10
0.20
0.30
0.40
0.50
PHI
Φ
UNIFORM DISTR
β_{d_1} = 1%
β_{s_1} = 5%
Re $\tilde{c}_{s_2}$
960
920
880
840
800
0.00
0.10
0.20
0.30
0.40
0.50
PHI
Φ
UNIFORM DISTR
β_{d_1} = 5%
β_{s_1} = 5%
Re $\tilde{c}_{s_2}$
960
920
880
840
800
0.00
0.10
0.20
0.30
0.40
0.50
PHI
Φ

FIGURE 8.

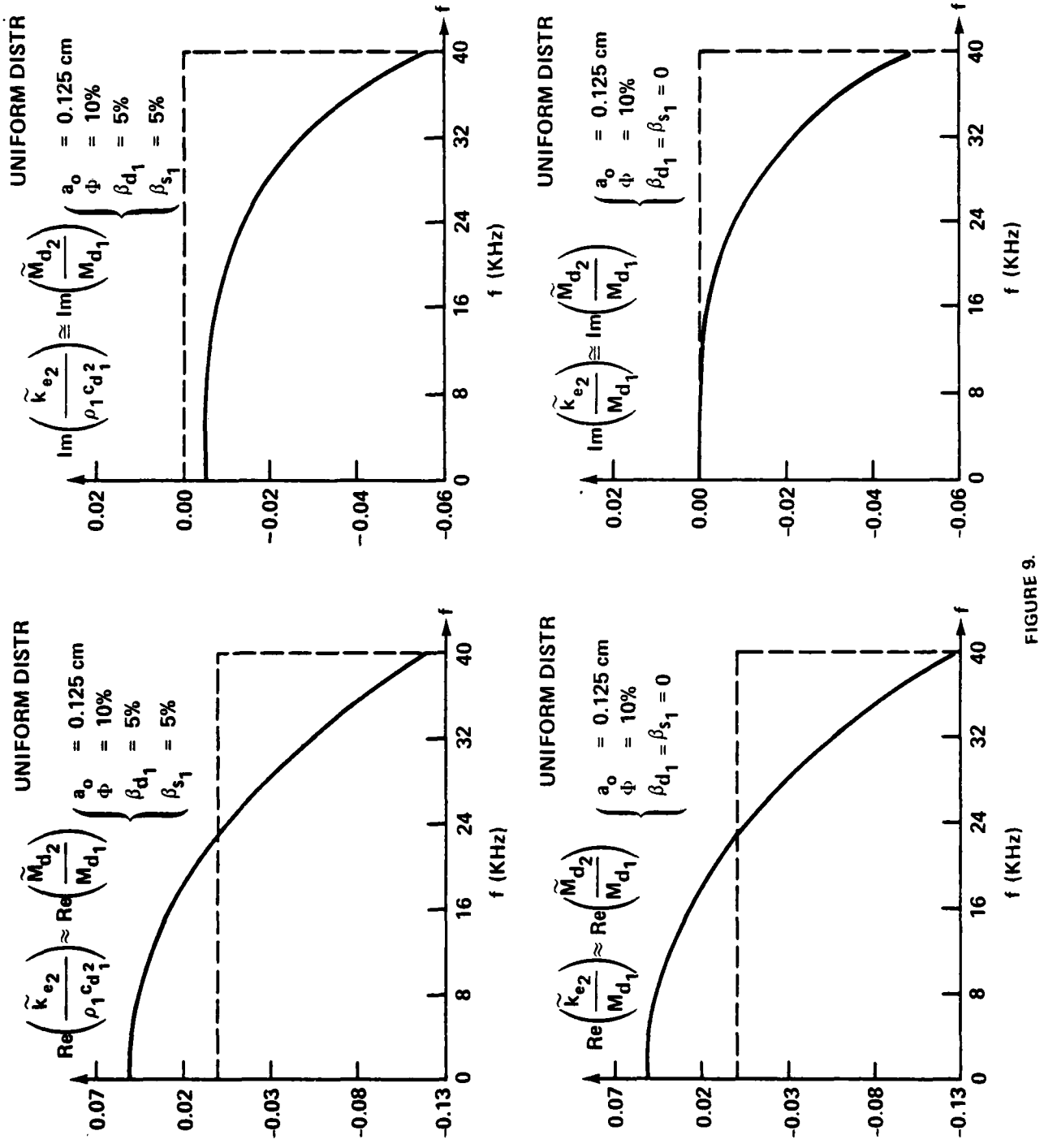
UNIFORM DISTR
$\mathrm{Re}\left(\frac{\tilde{k}_{e_2}}{\rho_1 c_{d_1}^2}\right) \approx \mathrm{Re}\left(\frac{\tilde{M}_{d_2}}{M_{d_1}}\right)$
a_o = 0.125 cm
Φ = 10%
β_{d_1} = 5%
β_{s_1} = 5%
0.07
0.02
-0.03
-0.08
-0.13
0
8
16
24
32
40
f (KHz)
f
UNIFORM DISTR
$\mathrm{Im}\left(\frac{\tilde{k}_{e_2}}{\rho_1 c_{d_1}^2}\right) \cong \mathrm{Im}\left(\frac{\tilde{M}_{d_2}}{M_{d_1}}\right)$
a_o = 0.125 cm
Φ = 10%
β_{d_1} = 5%
β_{s_1} = 5%
0.02
0.00
-0.02
-0.04
-0.06
0
8
16
24
32
40
f (KHz)
f
UNIFORM DISTR
$\mathrm{Re}\left(\frac{\tilde{k}_{e_2}}{M_{d_1}}\right) \approx \mathrm{Re}\left(\frac{\tilde{M}_{d_2}}{M_{d_1}}\right)$
a_o = 0.125 cm
Φ = 10%
$\beta_{d_1} = \beta_{s_1} = 0$
0.07
0.02
-0.03
-0.08
-0.13
0
8
16
24
32
40
f (KHz)
f
UNIFORM DISTR
$\mathrm{Im}\left(\frac{\tilde{k}_{e_2}}{M_{d_1}}\right) \cong \mathrm{Im}\left(\frac{\tilde{M}_{d_2}}{M_{d_1}}\right)$
a_o = 0.125 cm
Φ = 10%
$\beta_{d_1} = \beta_{s_1} = 0$
0.02
0.00
-0.02
-0.04
-0.06
0
8
16
24
32
40
f (KHz)
f

FIGURE 9.

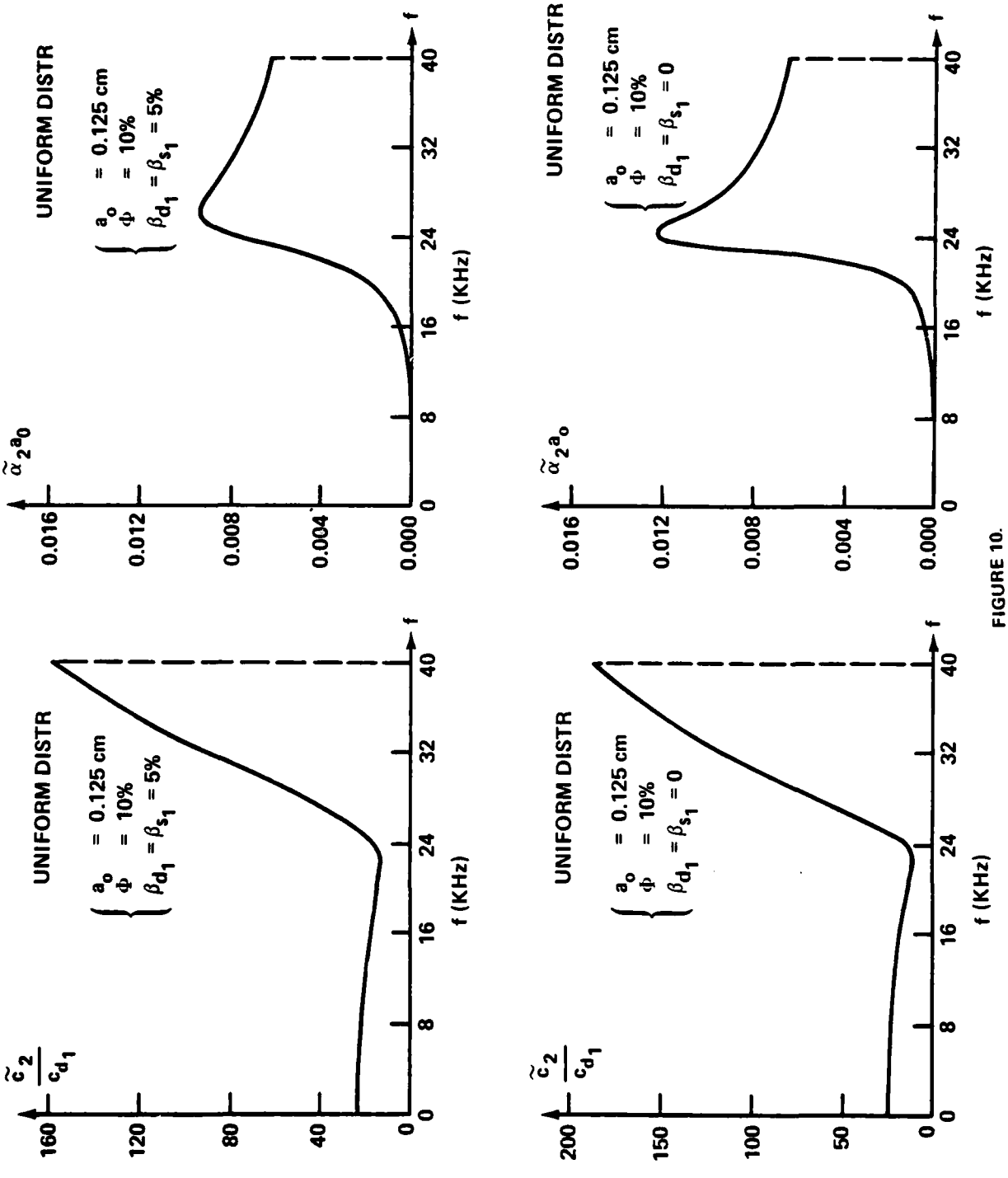
UNIFORM DISTR
a_o = 0.125 cm
Φ = 10%
$\beta_{d_1} = \beta_{s_1} = 5\%$
$\tilde{\alpha}_2 a_o$
0.016
0.012
0.008
0.004
0.000
0
8
16
24
32
40
f
f (KHz)
UNIFORM DISTR
a_o = 0.125 cm
Φ = 10%
$\beta_{d_1} = \beta_{s_1} = 0$
$\tilde{\alpha}_2 a_o$
0.016
0.012
0.008
0.004
0.000
0
8
16
24
32
40
f
f (KHz)
UNIFORM DISTR
a_o = 0.125 cm
Φ = 10%
$\beta_{d_1} = \beta_{s_1} = 5\%$
$\frac{\tilde{c}_2}{c_{d_1}}$
160
120
80
40
0
0
8
16
24
32
40
f
f (KHz)
UNIFORM DISTR
a_o = 0.125 cm
Φ = 10%
$\beta_{d_1} = \beta_{s_1} = 0$
$\frac{\tilde{c}_2}{c_{d_1}}$
200
150
100
50
0
0
8
16
24
32
40
f
f (KHz)

FIGURE 10.

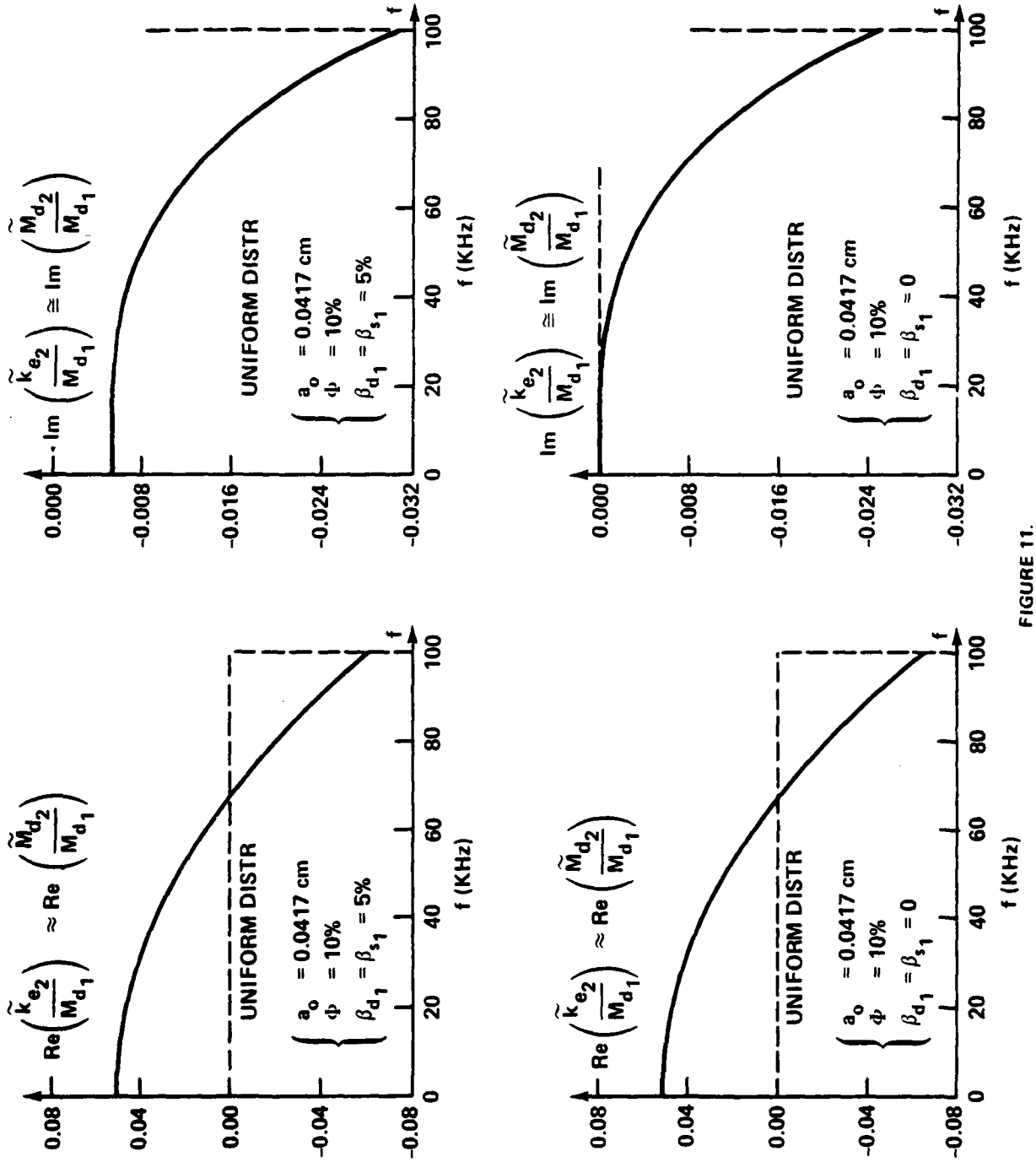
Im $\left(\frac{\tilde{k}_{e_2}}{M_{d_1}}\right) \cong$ Im $\left(\frac{\tilde{M}_{d_2}}{M_{d_1}}\right)$
Re $\left(\frac{\tilde{k}_{e_2}}{M_{d_1}}\right) \approx$ Re $\left(\frac{\tilde{M}_{d_2}}{M_{d_1}}\right)$
UNIFORM DISTR
a_o = 0.0417 cm
Φ = 10%
$\beta_{d_1} = \beta_{s_1}$ = 5%
$\beta_{d_1} = \beta_{s_1}$ = 0
f (KHz)
f

FIGURE 11.

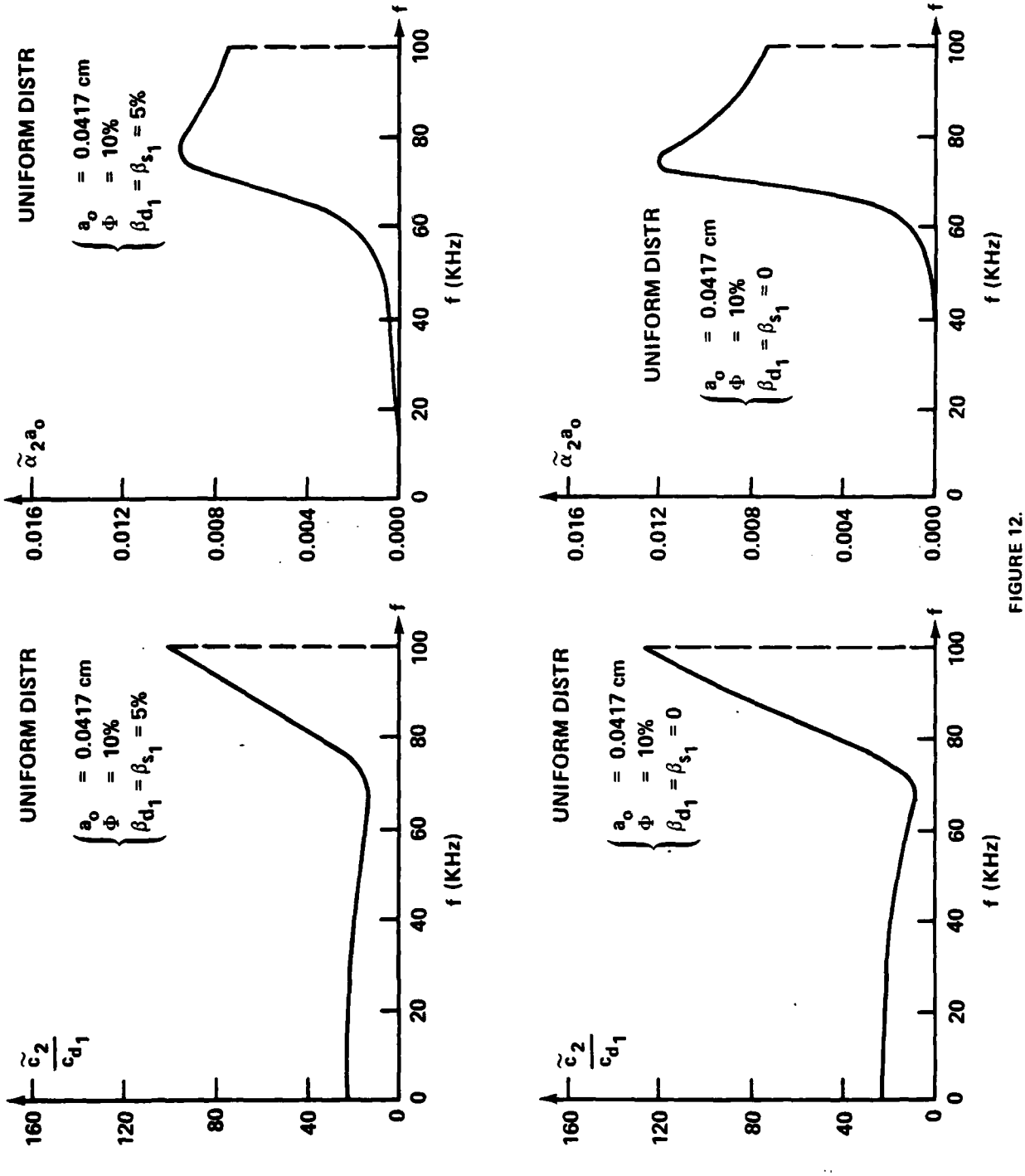
UNIFORM DISTR
$\begin{cases} a_o = 0.0417 \text{ cm} \\ \Phi = 10\% \\ \beta_{d_1} = \beta_{s_1} = 5\% \end{cases}$
$\tilde{\alpha}_2 a_o$
0.016
0.012
0.008
0.004
0.000
0
20
40
60
80
100
f (KHz)
f
UNIFORM DISTR
$\begin{cases} a_o = 0.0417 \text{ cm} \\ \Phi = 10\% \\ \beta_{d_1} = \beta_{s_1} = 0 \end{cases}$
$\frac{\tilde{c}_2}{c_{d_1}}$
160
120
80
40
0
0
20
40
60
80
100
f (KHz)
f

FIGURE 12.

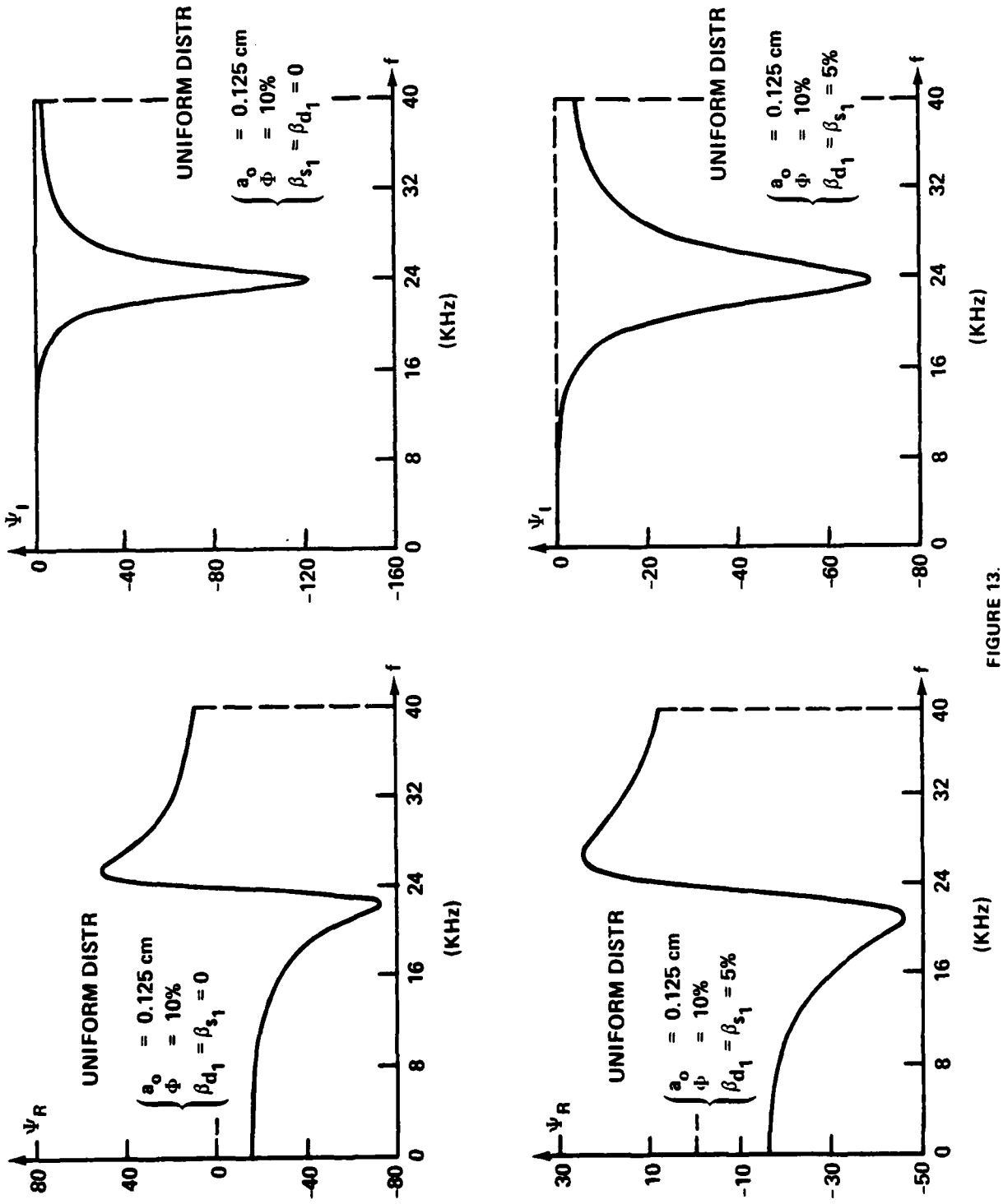
UNIFORM DISTR
$\begin{cases} a_o = 0.125\ cm \\ \Phi = 10\% \\ \beta_{d_1} = \beta_{s_1} = 0 \end{cases}$
Ψ_R
80
40
0
-40
-80
0
8
16
24
32
40
f
(KHz)
UNIFORM DISTR
$\begin{cases} a_o = 0.125\ cm \\ \Phi = 10\% \\ \beta_{s_1} = \beta_{d_1} = 0 \end{cases}$
Ψ_I
0
-40
-80
-120
-160
0
8
16
24
32
40
f
(KHz)
UNIFORM DISTR
$\begin{cases} a_o = 0.125\ cm \\ \Phi = 10\% \\ \beta_{d_1} = \beta_{s_1} = 5\% \end{cases}$
Ψ_R
30
10
-10
-30
-50
0
8
16
24
32
40
f
(KHz)
UNIFORM DISTR
$\begin{cases} a_o = 0.125\ cm \\ \Phi = 10\% \\ \beta_{d_1} = \beta_{s_1} = 5\% \end{cases}$
Ψ_I
0
-20
-40
-60
-80
0
8
16
24
32
40
f
(KHz)

FIGURE 13.

$$n \equiv \left[\frac{N}{\frac{4\pi}{3} R^3}\right]; \quad \Phi \equiv \frac{4\pi}{3} \int_{-\infty}^{+\infty} g(a)\, a^3\, da = \frac{3}{2}\left(\frac{Na_o^3}{R^3}\right)$$

TRIANGULAR DISTRIBUTION FUNCTION: g(a)

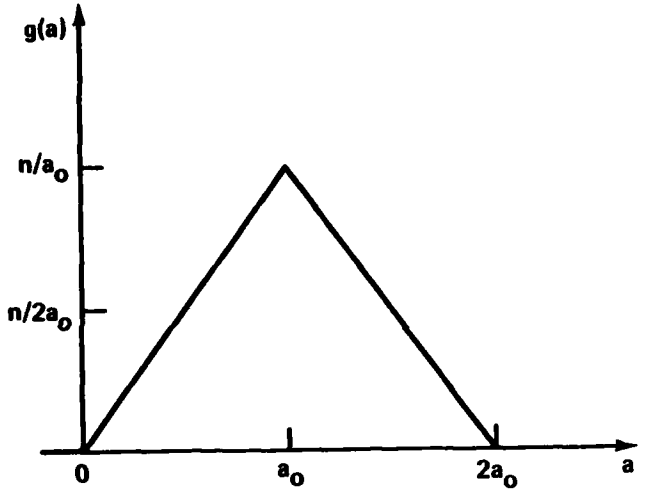

$$g(a) \equiv \begin{cases} \frac{na}{a_o^2} & (0 \leq a \leq a_o) \\ \frac{2n}{a_o} - \frac{an}{a_o^2} & (a_o \leq a \leq 2a_o) \\ 0 & \text{(ELSEWHERE)} \end{cases}$$

CUMULATIVE TRIANGULAR DISTRIBUTION FUNCTION

$$Q(a) = \frac{1}{n} \int_{-\infty}^{+\infty} g(a)da$$

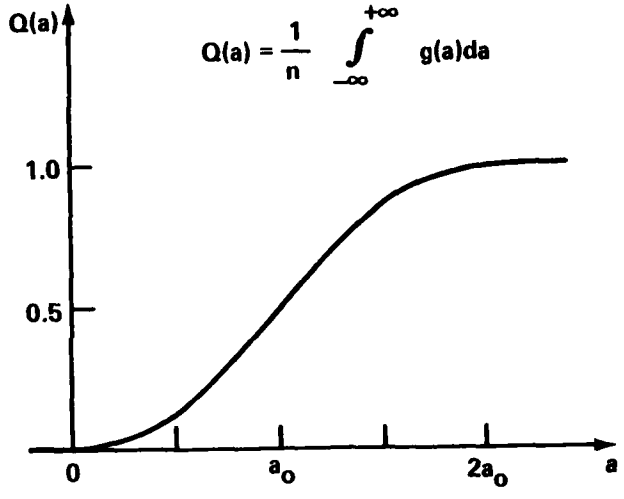

$$Q(a) \equiv \begin{cases} \frac{a^2}{2a_o^2} & (0 \leq a \leq a_o) \\ \frac{1}{2} + \frac{1}{2a_o}(a - a_o)(3a_o - a) & \\ 1 & (a \geq 2a_o) \end{cases}$$

FIGURE 14.

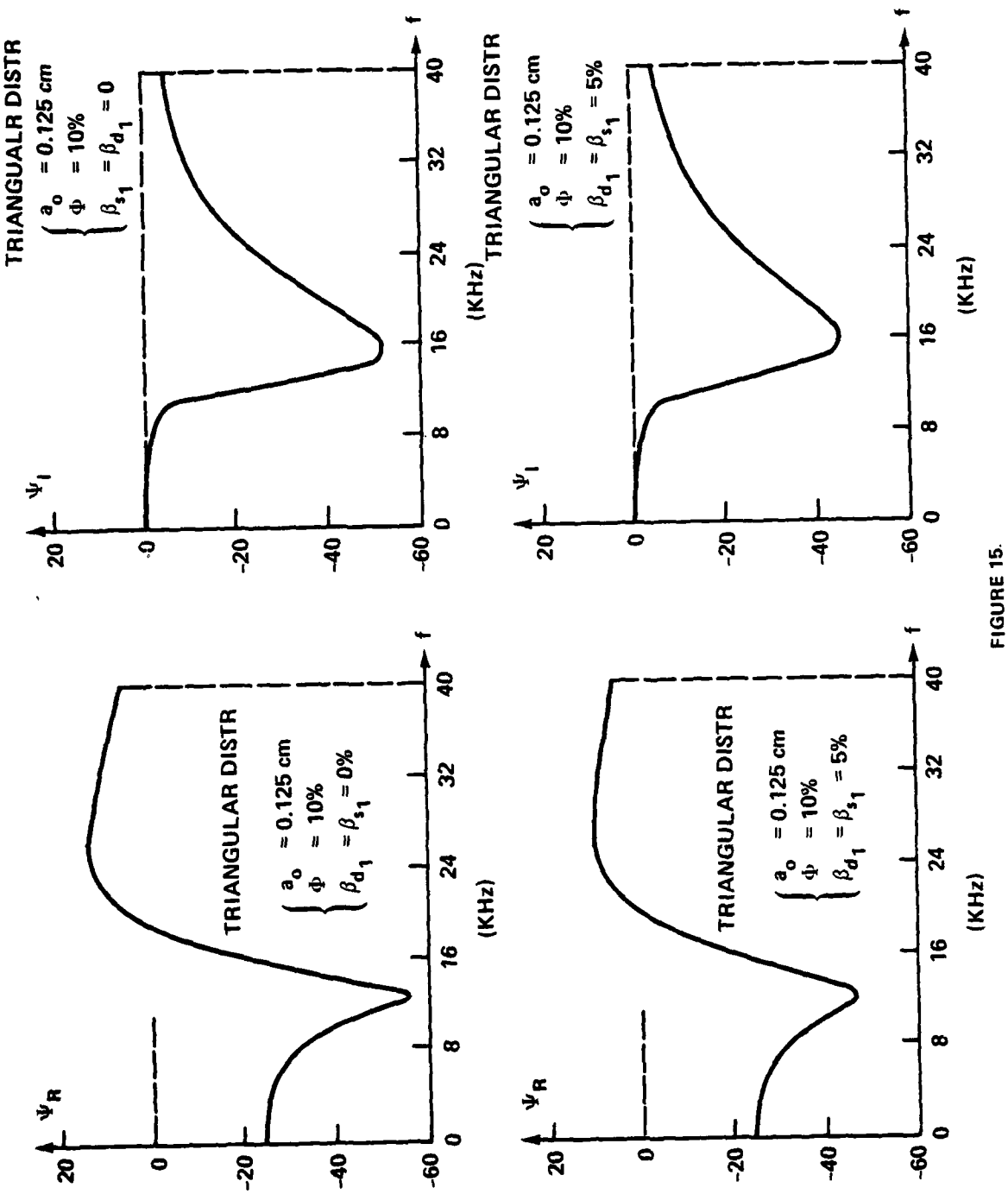
TRIANGUALR DISTR
a_o = 0.125 cm
Φ = 10%
$\beta_{s_1} = \beta_{d_1} = 0$
TRIANGULAR DISTR
a_o = 0.125 cm
Φ = 10%
$\beta_{d_1} = \beta_{s_1} = 5\%$
TRIANGULAR DISTR
a_o = 0.125 cm
Φ = 10%
$\beta_{d_1} = \beta_{s_1} = 0\%$
TRIANGULAR DISTR
a_o = 0.125 cm
Φ = 10%
$\beta_{d_1} = \beta_{s_1} = 5\%$
Ψ_I
Ψ_R
20
0
-20
-40
-60
0
8
16
24
32
40
f
(KHz)

FIGURE 15.

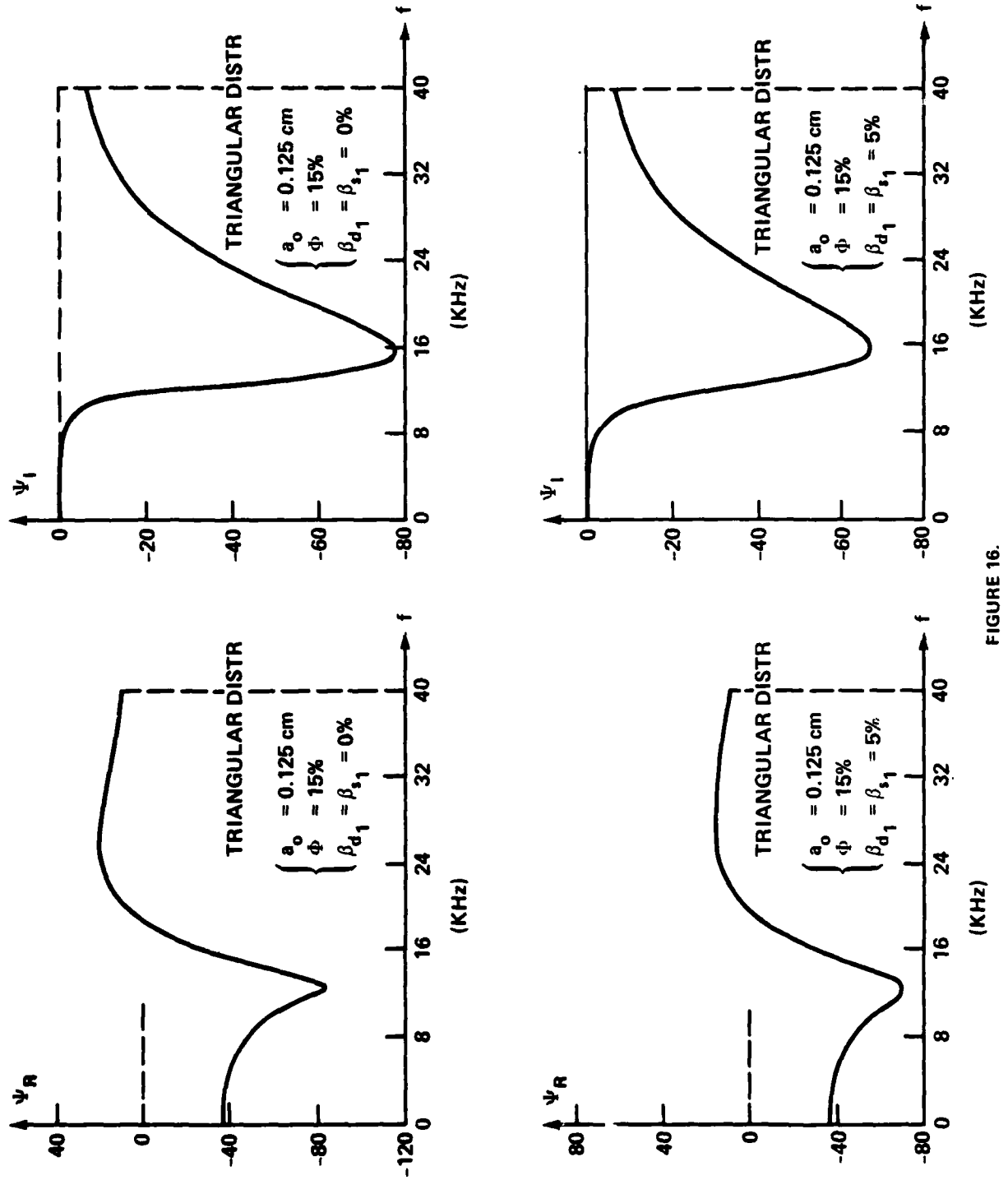
TRIANGULAR DISTR
a_o = 0.125 cm
Φ = 15%
$\beta_{d_1} = \beta_{s_1}$ = 0%
$\beta_{d_1} = \beta_{s_1}$ = 5%
Ψ_I
Ψ_R
f
(KHz)

FIGURE 16.

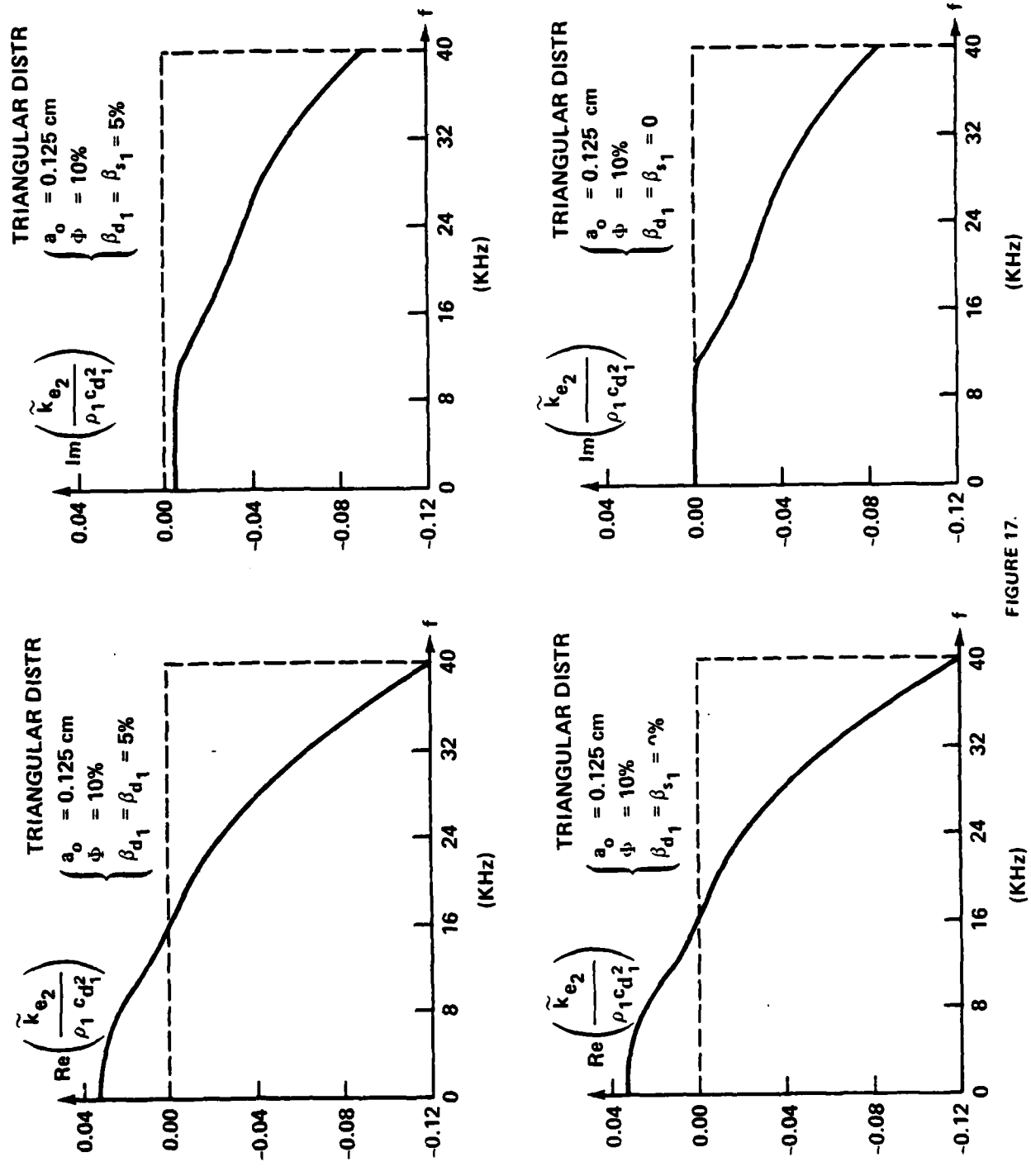
TRIANGULAR DISTR
a_o = 0.125 cm
Φ = 10%
$\beta_{d_1} = \beta_{s_1} = 5\%$
$\beta_{d_1} = \beta_{s_1} = 0$
$\beta_{d_1} = \beta_{s_1} = 5\%$
$\beta_{d_1} = \beta_{s_1} = 0$
$\mathrm{Re}\left(\frac{\tilde{k}_{e_2}}{\rho_1 c_{d_1}^2}\right)$
$\mathrm{Im}\left(\frac{\tilde{k}_{e_2}}{\rho_1 c_{d_1}^2}\right)$
0.04
0.00
-0.04
-0.08
-0.12
0
8
16
24
32
40
f
(KHz)

FIGURE 17.

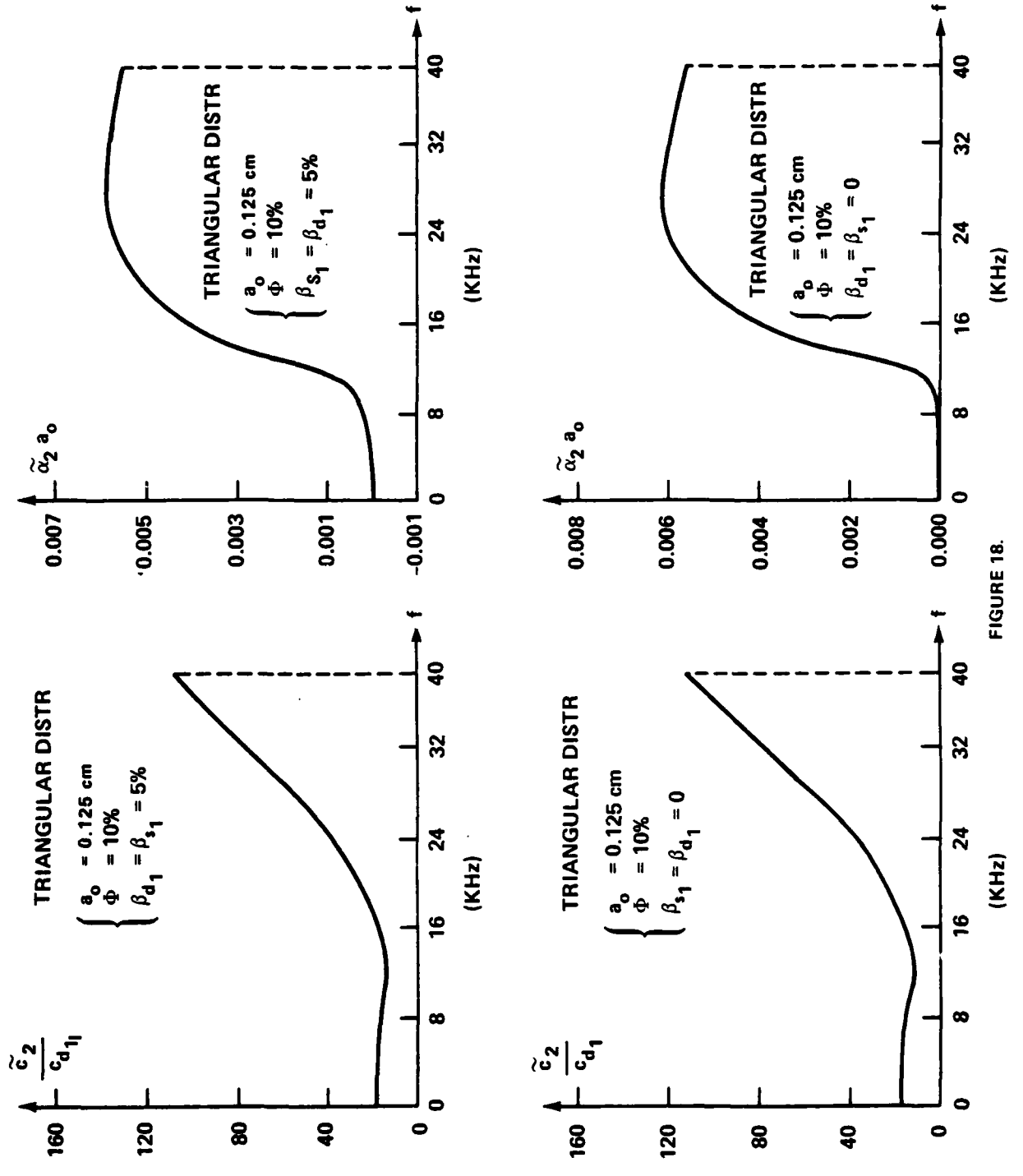
TRIANGULAR DISTR
a_o = 0.125 cm
Φ = 10%
$\beta_{d_1} = \beta_{s_1}$ = 5%
$\frac{\tilde{c}_2}{c_{d_{11}}}$
160
120
80
40
0
0
8
16
24
32
40
f
(KHz)
TRIANGULAR DISTR
a_o = 0.125 cm
Φ = 10%
$\beta_{s_1} = \beta_{d_1}$ = 5%
$\tilde{\alpha}_2 a_o$
0.007
0.005
0.003
0.001
-0.001
0
8
16
24
32
40
f
(KHz)
TRIANGULAR DISTR
a_o = 0.125 cm
Φ = 10%
$\beta_{s_1} = \beta_{d_1}$ = 0
$\frac{\tilde{c}_2}{c_{d_1}}$
160
120
80
40
0
0
8
16
24
32
40
f
(KHz)
TRIANGULAR DISTR
a_o = 0.125 cm
Φ = 10%
$\beta_{d_1} = \beta_{s_1}$ = 0
$\tilde{\alpha}_2 a_o$
0.008
0.006
0.004
0.002
0.000
0
8
16
24
32
40
f
(KHz)

FIGURE 18.

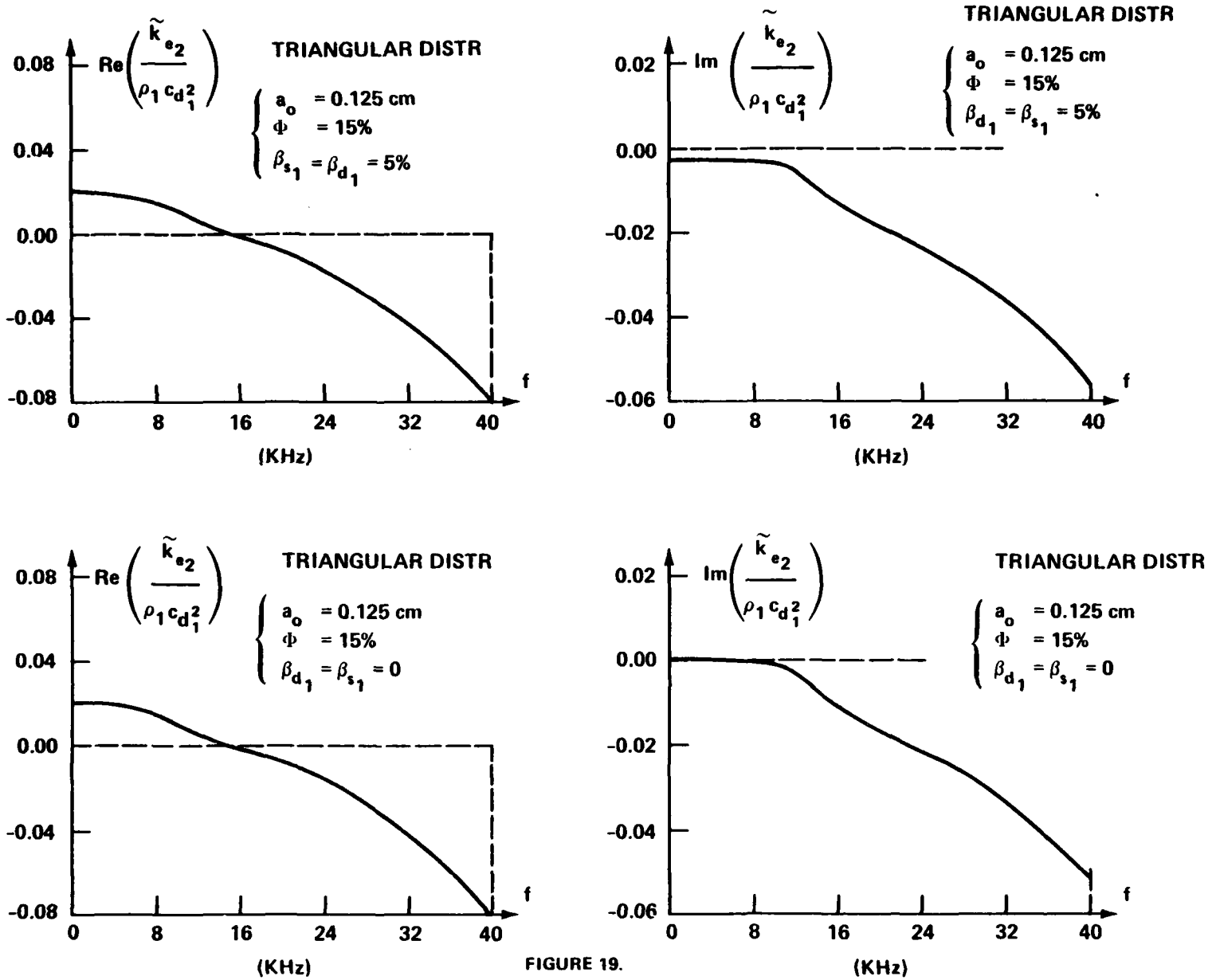
TRIANGULAR DISTR
a_o = 0.125 cm
Φ = 15%
$\beta_{s_1} = \beta_{d_1}$ = 5%
$\mathrm{Re}\left(\frac{\tilde{k}_{e_2}}{\rho_1 c_{d_1}^2}\right)$
$\mathrm{Im}\left(\frac{\tilde{k}_{e_2}}{\rho_1 c_{d_1}^2}\right)$
0.08
0.04
0.00
-0.04
-0.08
0.02
-0.02
-0.06
0
8
16
24
32
40
f
(KHz)
$\beta_{d_1} = \beta_{s_1}$ = 0

FIGURE 19.

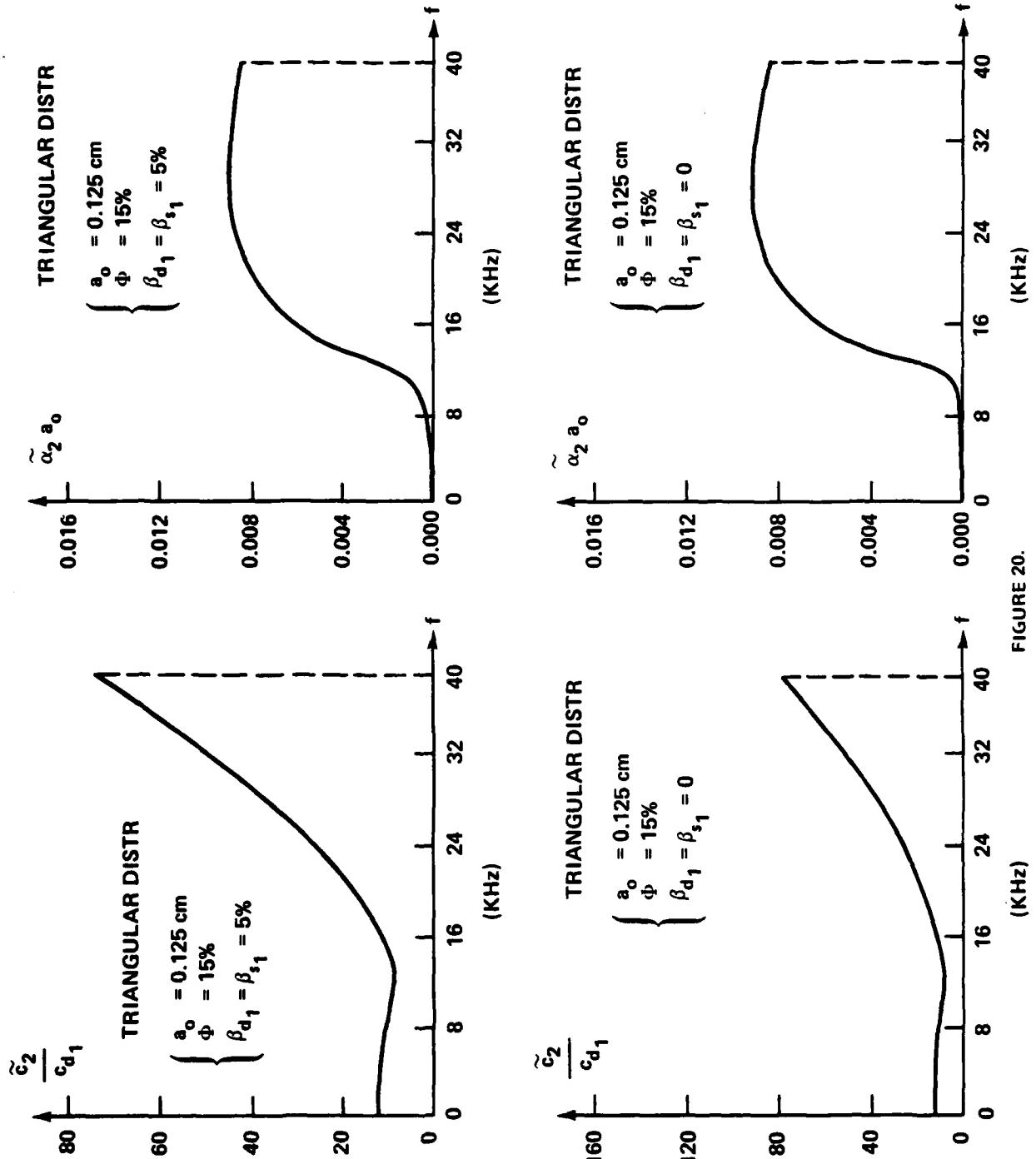
TRIANGULAR DISTR
a_o = 0.125 cm
Φ = 15%
$\beta_{d_1} = \beta_{s_1} = 5\%$
$\beta_{d_1} = \beta_{s_1} = 0$
$\tilde{\alpha}_2 a_o$
$\frac{\tilde{c}_2}{c_{d_1}}$
f
(KHz)
0.016
0.012
0.008
0.004
0.000
160
120
80
40
0
8
16
24
32
40

FIGURE 20.

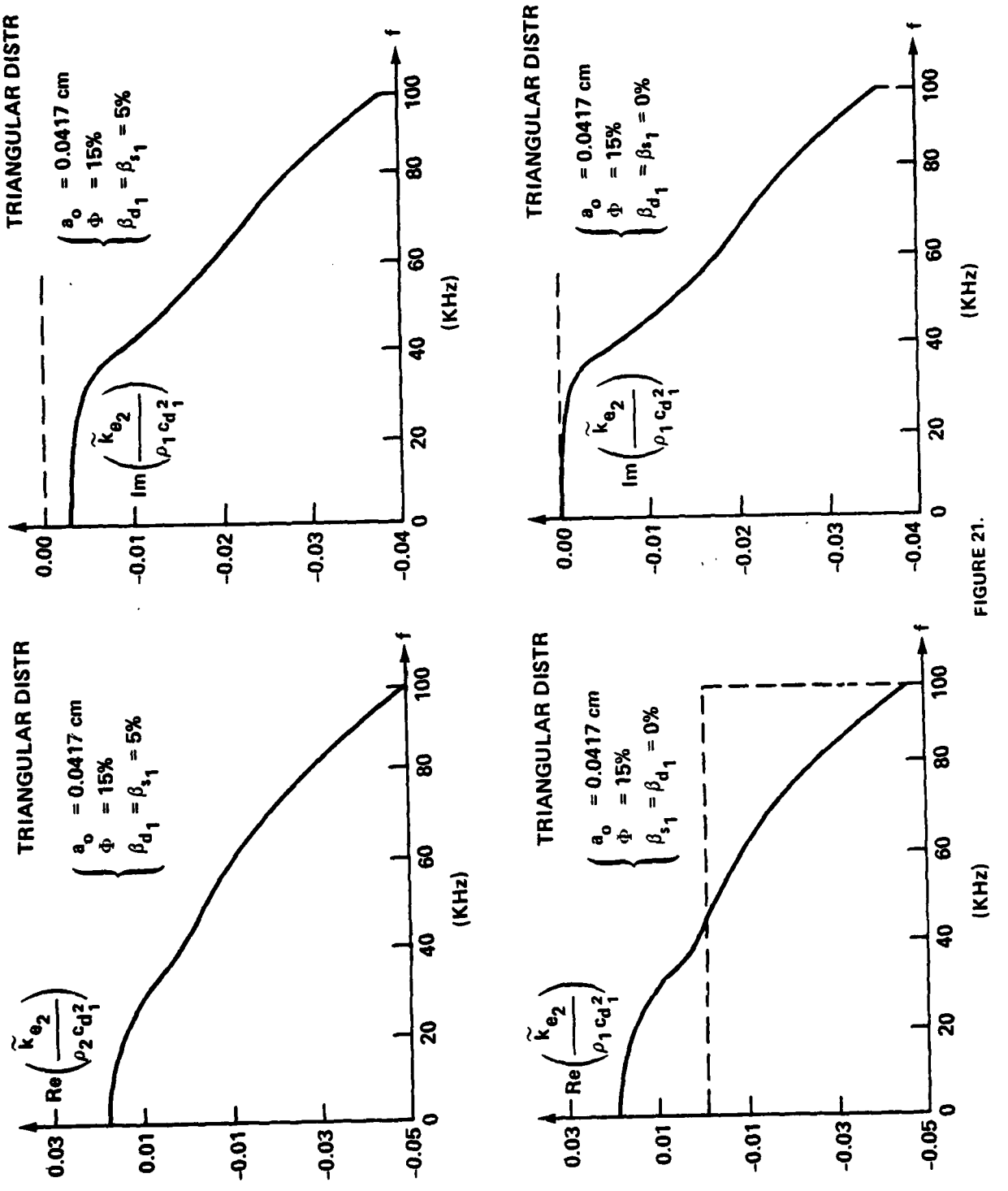
TRIANGULAR DISTR
a_o = 0.0417 cm
Φ = 15%
$\beta_{d_1} = \beta_{s_1}$ = 5%
$\beta_{d_1} = \beta_{s_1}$ = 0%
$\beta_{s_1} = \beta_{d_1}$ = 0%
$\mathrm{Re}\left(\frac{\tilde{k}_{e_2}}{\rho_2 c_{d_1}^2}\right)$
$\mathrm{Im}\left(\frac{\tilde{k}_{e_2}}{\rho_1 c_{d_1}^2}\right)$
f
(KHz)
0.03
0.01
-0.01
-0.03
-0.05
0.00
-0.04
0
20
40
60
80
100

FIGURE 21.

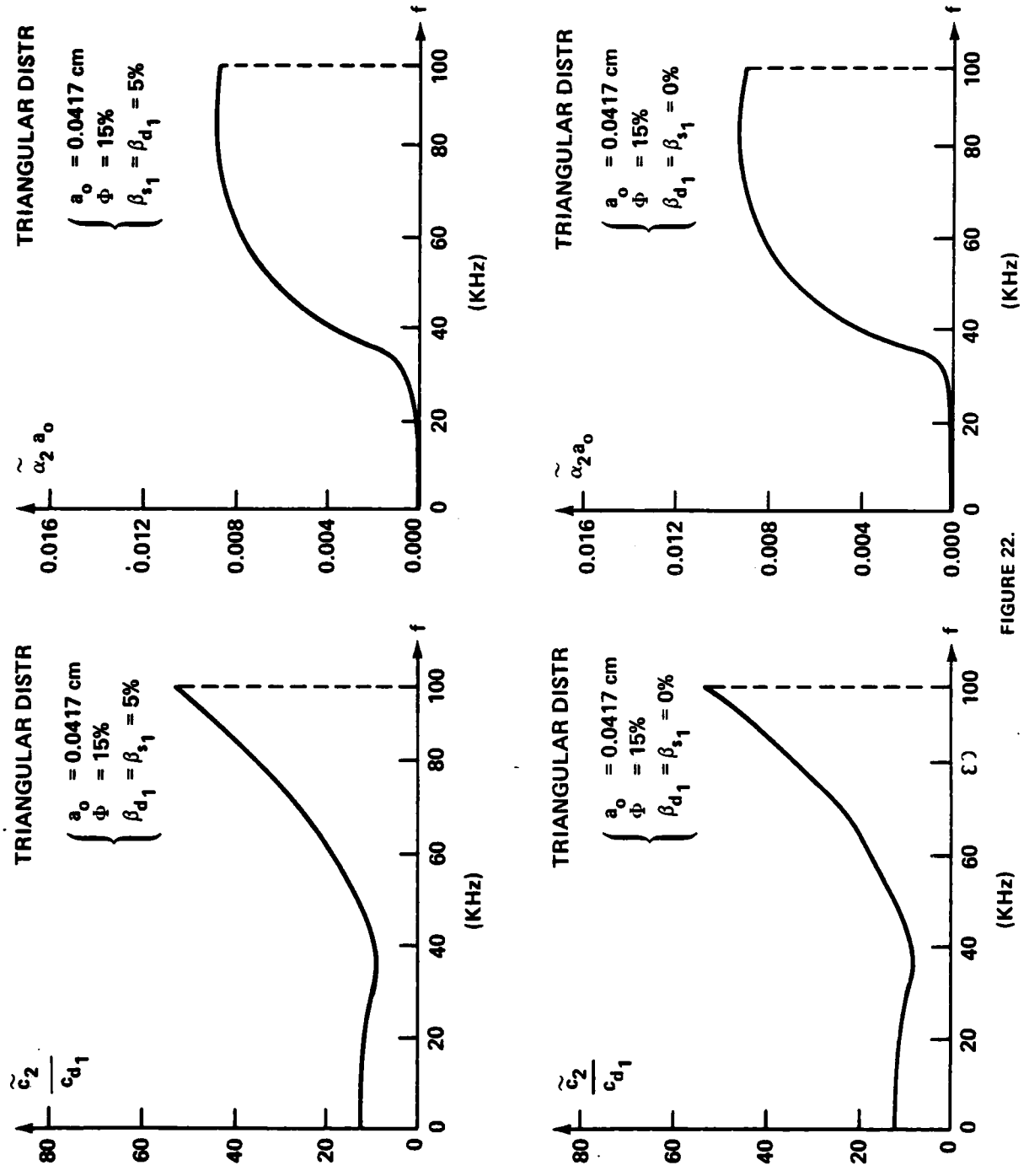
TRIANGULAR DISTR
a_o = 0.0417 cm
Φ = 15%
$\beta_{s_1} = \beta_{d_1}$ = 5%
$\tilde{\alpha}_2 a_o$
0.016
0.012
0.008
0.004
0.000
0
20
40
60
80
100
f
(KHz)
TRIANGULAR DISTR
a_o = 0.0417 cm
Φ = 15%
$\beta_{d_1} = \beta_{s_1}$ = 0%
$\tilde{\alpha}_2 a_o$
0.016
0.012
0.008
0.004
0.000
0
20
40
60
80
100
f
(KHz)
TRIANGULAR DISTR
a_o = 0.0417 cm
Φ = 15%
$\beta_{s_1} = \beta_{d_1}$ = 5%
$\frac{\tilde{c}_2}{c_{d_1}}$
80
60
40
20
0
0
20
40
60
80
100
f
(KHz)
TRIANGULAR DISTR
a_o = 0.0417 cm
Φ = 15%
$\beta_{d_1} = \beta_{s_1}$ = 0%
$\frac{\tilde{c}_2}{c_{d_1}}$
80
60
40
20
0
0
20
40
60
80
100
f
(KHz)

FIGURE 22.

REFERENCES

1. G. Gaunaurd and H. Überall, "Resonance Theory of the Effective Properties of Perforated Solids," J. of the Acoustical Soc. America, Vol. 71, No. 2, 1982, pp. 282-295.

2. G. Gaunaurd, "Methods For Solving the Viscoelastic Equations For Cylinder and Sphere Problems," NSWC TR 76-20, 22 Mar 1976, 28 pp., (ADA025302).

3. G. Gaunaurd and H. Überall, "Theory of Resonant Scattering From Spherical Cavities in Elastic and Viscoelastic Media," J. Acoustical Society of America, Vol. 63, 1978, pp. 1699-1712.

4. G. Gaunaurd and H. Überall, "Resonance Theory of Bubbly Liquids," J. of the Acoustical Soc. America, Vol. 69, 1981, pp. 362-370.

5. G. Gaunaurd and H. Überall, "Errata: Resonance Theory of the Effective Properties of Perforated Solids," J. of the Acoustical Soc. America (to be published), 1983.

6. G. Gaunaurd, et al., "New Method To Determine Shear Absorption Using the Viscoelastodynamic Resonance Scattering Formalism," J. of the Acoustical Soc. America, Vol. 64, 1978, pp. 1211-1212.

7. G. Gaunaurd, et al., "Giant Monopole Resonances in the Scattering of Waves From Gas-filled Spherical Cavities and Bubbles," J. of the Acoustical Soc. America, Vol. 65, 1979, pp. 573-594.

8. E. H. Kerner, "The Elastic and Thermoelastic Properties of Composite Media," Proc. Phys. Soc. (London), Vol. 69B, 1956, pp. 808-813.

9. I. A. Chaban, Soviet Phys. - Acoustics, Vol. 10, 1965, pp. 298-304, and, Vol. 11, 1965, pp. 81-86.

10. R. L. Kligman, et al., "Effective Dynamic Properties of Composite Viscoelastic Materials," J. of the Acoustical Soc. America, Vol. 70, 1981, pp. 1437-1444.

11. N. Yamakawa, "Scattering and Attenuation of Elastic Waves, Parts I and II," Geophys. Magaz. (Tokyo), Vol. 31, 1962, pp. 63-103.

12. E. Meyer, et al., "P[illegible]sation Oscillations of Cavities in Rubber," J. of the Acoustical Soc. America, Vol. 30, 1958, pp. 1116-1124.

13. R. M. Christensen, Mechanics of Composite Materials, J. Wiley & Sons, New York, 1979, p. 60.

PROGRAM LOOK 73/74 OPT=1 FTN 4.6+433 87/38/82 18.33.24


```
      PROGRAM LOOK(INPUT,OUTPUT)
      COMMON /PTS/ M,XX( 512),YY( 512)
      DIMENSION VV1( 512)
      DIMENSION VV2( 512),VV3( 512)
      DIMENSION FMT(5)
      DIMENSION RADIUS(4),PHIS(4),FREQS(4)
      DIMENSION BSS(3),BDD(3)
      COMPLEX PSI,BULK,SQUAT
      REAL KAY
      DATA RADIUS/2.E-4,2.E-4,20.E-4,20.E-4/
      DATA PHIS/.05,.10,.05,.10/
      DATA FREQS/100.E6,100.E6,50.E6,50.E6/
      DATA BSS/.05,.05,.05/
      DATA BDD/.01,.02,.05/
C
C
C
      PI=3.1415926536
      RHO1=1.13
      RHO2=.0012
      P1CD12=2.215E10
      P1CS12=.81E10
      P2CD22=1.42E6
      P2CS22=0.0
      CD1=1.40E5
C
      Q1=P1CD12/P2CD22
      Q2=(4.0/3.0)*P1CS12/P2CD22
      Q3=(4./3.)*P1CS12/P1CD12
      PTS=300.
      PTS=500.
      MAX=PTS
      LBSTA=1
      LBEND=3
      DO 2000 LBS=LBSTA,LBEND
      BS1=BSS(LBS)
      BD1=BDD(LBS)
      BD124=4.*BD1*BD1
      KSTART=1
      KEND=4
      DO 1000 KASE=KSTART,KEND
      PHI=PHIS(KASE)
      A=RADIUS(KASE)
      AA=A*1.E4
      ENCODE(44,215,FMT)AA,PHI,BS1,BD1
  215 FORMAT(' A=',F6.2,' MICRONS',',',PHI=',F4.2,',BS1=',F4.2,',BD1=',
     1    F4.2)
      PRINT 215,AA,PHI,BS1,BD1
      FMAX=FREQS(KASE)
      DELTA=FMAX/PTS
      M=0
      F=DELTA
      DO 50 I=1,MAX
      M=M+1
      AF=(((PI+PI)*A*F)/CD1)
      AF2=AF*AF
      AF3=AF2*AF
```

```
      C
      C     BEGIN EQUATIONS
   60 C
            G= 1. - Q1 + Q2
            H=(Q1*2.*BD1) - (Q2*2.*BS1)
            P=1. + Q2 - (Q1*AF2/3.) + ((Q1*AF3/3.)*
           1     SQRT( (SQRT(1.+BD124)-1.)/(2.*(1.+BD124))))
   65       Q=((-Q1*AF3/3.)*SQRT( (SQRT(1.+BD124)+1.)/
           1     (2.*(1.+BD124)))) - (Q2*2.*BS1)
            PSI=PHI*(CMPLX(G,H)/CMPLX(P,Q))
            PSIR=REAL(PSI)
            PSII=AIMAG(PSI)
   70       X=1. - PSIR
            Y=-PSII
            EM=((9.*P1CD12 - 4.*P1CS12) + ((BS1+BS1)*
           1     (-18.*P1CD12*BD1 + 8.*P1CS12*BS1))) * (1.-PHI)
            EN=(-18.*P1CD12*BD1 + 8.*P1CS12*BS1 -
   75      1     ((BS1+BS1)*(9.*P1CD12 - 4.*P1CS12))) * (1.-PHI)
            KAY=9.*P1CD12 - 4.*P1CS12 + ((6.*P1CD12 + 4.*P1CS12)*PHI)
            ELL=-18.*P1CD12*BD1 + 8.*P1CS12*BS1
           1     -((BS1+BS1)*(9.*P1CD12 - 4.*P1CS12)*PHI)
            P1=KAY**2 + ELL**2
   80       P2=1. - (((EM*KAY) + (EN*ELL))/P1)
            P3=(BS1+BS1) + (((EN*KAY) - (EM*ELL))/P1)
            U=1. - (Q3*((P2*(1.-PSIR)) - (P3*PSII)))
            V=(Q3*((P2*PSII) + (P3*(1.-PSIR)))) - (BS1+BD1)
            SP=U**2 + V**2
   85       S1=SP + SP
            S2=SQRT(SP*(X**2 + Y**2))
            S3=X*U + Y*V
            S4=(1./SQRT(1.-(1.-((RHO2/RHO1)*PHI))))
            YY(M)=S4*SQRT(S1/(S2+S3))
   90       YY1(M)=-AF*(PSII/ABS(PSII))    *SQRT((S2-S3)/S1)/S4
            XX(M)=F*1.E-6
            F=F+DELTA
      50    CONTINUE
            XX(M+1)=0.0
   95       XX(M+2)=FMAX/5.EE
            PRINT 20,(XX(J),YY(J),J=1,M)
      20    FORMAT( 5(*  X=*, F7.3,*,Y=*,E10.4))
            CALL CCMPLT( 10H F(MEGHZ) ,10HC20AR/CD1  ,FMT, 44)
            DO 400 J=1,M
  100       YY(J)=YY1(J)
      400   CONTINUE
            PRINT 20,(XX(J),YY(J),J=1,M)
             CALL COMPLT( 10H F(MEGHZ) ,10HALPHA2BAR  ,FMT, 44)
      1000  CONTINUE
  105 .     2000 CONTINUE
            CALL PLOTFIN
            END
```

SYMBOLIC REFERENCE MAP (R=2)

PROGRAM UNIT 74/74 OPT=1 FTN 4.6+433 07/23/82 16.00.06 PAGE 3

VARIABLES		SN	TYPE	RELOCATION						
					DEFINED	36						
4515	BULK		COMPLEX		REFS	8	60	61	62	63		
					DEFINED	59						
4531	C01	*	REAL		DEFINED	25						
4546	DELTA		REAL		REFS	45	72	DEFINED	44			
4553	ELL		REAL		REFS	59	DEFINED	57				
4551	EM		REAL		REFS	59	DEFINED	52				
4552	EN		REAL		REFS	59	DEFINED	54				
7562	FNT		REAL	ARRAY	REFS	5	78	83	88	93		
					DEFINED	39						
7577	FREQS		REAL	ARRAY	REFS	6	DEFINED	12				
4550	I	*	INTEGER		DEFINED	47						
4561	J		INTEGER		REFS	2*76	2*80	2*82	2*85	2*87	2*90	2*92
					DEFINED	76	79	82	84	87	89	92
4521	KAY		REAL		REFS	9	59	DEFINED	56			
4540	LOUND		INTEGER		REFS	35	DEFINED	34				
4541	LPS		INTEGER		REFS	36	37	DEFINED	35			
4537	LASTA		INTEGER		REFS	35	DEFINED	33				
0	M		INTEGER	PTS	REFS	2	48	60	61	69	70	71
						74	75	76	79	82	84	87	89
						92	DEFINED	46	48				
4536	MAX		INTEGER		REFS	47	DEFINED	32				
4547	PHI		REAL		REFS	52	54	56	57	68	71	72
					DEFINED	45	72					
4545	PHIMAX		REAL		REFS	44	75	DEFINED	43			
7573	PHIS		REAL	ARRAY	REFS	6	DEFINED	11				
4522	PI	*	REAL		DEFINED	18						
4513	PLT	*	COMPLEX	*UNDEF	REFS	8						
4535	PTS		REAL		REFS	32	44	DEFINED	30	31		
4525	P1CD12		REAL		REFS	27	29	2*52	2*54	2*56	2*57	
					DEFINED	21						
4526	P1CS12		REAL		REFS	28	29	2*52	2*54	2*56	2*57	
					DEFINED	22						
4527	P2CD22		REAL		REFS	27	28	DEFINED	23			
4530	P2CS22	*	REAL		DEFINED	24						
4532	Q1	*	REAL		DEFINED	27						
4533	Q2	*	REAL		DEFINED	26						
4534	Q3	*	REAL		DEFINED	29						
7567	RADIUS		REAL	ARRAY	REFS	6	DEFINED	10				
4557	RCX		REAL		REFS	67	DEFINED	65				
4560	RCY		REAL		REFS	67	DEFINED	66				
4523	RHO1		REAL		REFS	2*68	DEFINED	19				
4524	RHO2		REAL		REFS	66	DEFINED	20				
4554	RX		REAL		REFS	64	65	66	DEFINED	62		
4555	RY		REAL		REFS	64	2*66	DEFINED	63			
4556	R1		REAL		REFS	65	66	DEFINED	64			
4517	SQUAT		COMPLEX		REFS	6	68	69	70	DEFINED	67	68
1	XX		REAL	ARRAY PTS	REFS	2	76	82	87	92		
					DEFINED	71	74	75				
1001	YY		REAL	ARRAY PTS	REFS	2	76	82	87	92		
					DEFINED	60	80	85	90			
4562	YY1		REAL	ARRAY	REFS	3	80	DEFINED	61			
5562	YY2		REAL	ARRAY	REFS	4	65	DEFINED	69			
6562	YY3		REAL	ARRAY	REFS	4	90	DEFINED	70			

PROGRAM LOOK 74/74 OPT=1 FTN 4.6+433 07/28/82 16.00.06

```
FILE NAMES          MODE
    0  INPUT
 2043  OUTPUT       FMT                 WRITES      42        76        82        87        92

EXTERNALS           TYPE    ARGS        REFERENCES
       COMPLT                4           78        83        88        93
       PLOTFIN               0           86
       SQRT         REAL     1 LIBRARY   64        65        66        68

INLINE FUNCTIONS    TYPE    ARGS        DEF LINE  REFERENCES
       ABS          REAL     1  INTRIN              66
       AIMAG        REAL     1  INTRIN              61        63        70
       CMPLX        COMPLEX  2  INTRIN              2*59      67
       REAL         REAL     1  INTRIN              60        62        69

STATEMENT LABELS                DEF LINE  REFERENCES
 4436  20           FMT          77        76        82        87        92
    0  50                        73        47
 4416  215          FMT          40        39        42
    0  400                       81        79
    0  500                       86        84
    0  600                       91        89
    0  1000         INACTIVE     94
    0  2000                      95        35

LOOPS  LABEL    INDEX      FROM-TO    LENGTH    PROPERTIES
 4137  2000   * LBS          35 95      2238              EXT REFS  NOT INNER
 4155  50     * I            47 73       66B              EXT REFS
 4250          * J            76 76       10B              EXT REFS
 4266  400       J            79 81       3B     INSTACK
 4274          * J            82 82       10B              EXT REFS
 4312  500       J            84 86       3B     INSTACK
 4320          * J            87 87       10B              EXT REFS
 4336  600       J            89 91       3B     INSTACK
 4344          * J            92 92       10B              EXT REFS

COMMON BLOCKS    LENGTH
       PTS         1025

STATISTICS
  PROGRAM LENGTH                35238    1875
  BUFFER LENGTH                 41068    2118
  CM LABELED COMMON LENGTH      2001B    1025
```

SUBROUTINE COMPLT 73/74 OPT=1 FTN 4.6+433

```
      SUBROUTINE COMPLT(XTITLE,YTITLE,TITLE,LEN)
      COMMON /PTS/ N,X( 512),Y( 512)
      DIMENSION IB(1000)
      DATA JOY/0/,NGPH/0/
      DATA AX/ 5./,AY/4./,DELY/4./
      JOY=JOY+1
      IF(JOY.NE.1) GOTO 1
      CALL PLOTS(IB,1000,13)
      CALL FACTOR(.25)
      CALL CCIDNT(0.,9,9H NOO A114 )
      CALL FACTOR(1.0)
      CALL PLOT(2.,2.,-3)
    1 CONTINUE
      NGPH=NGPH+1
      IF(NGPH.LT.5)  GO TO 5
      YP=-((NGPH-1)*(AY+DELY) )
      CALL PLOT(AX+6.,YP,-3)
      NGPH=1
    5 CONTINUE
C   DRAW VERTICAL AXIS
C
      CALL SCALE(Y,AY,N,1)
      CALL AXIS(0.,0.,YTITLE,10,AY,90.,Y(N+1),Y(N+2))
C
C   DRAW HORIZONTAL AXIS
C
      CALL AXIS(0.0,0.0,XTITLE,-10,AX,0.0,X(N+1),X(N+2))
C
C
      CALL LINE(X,Y,N,1,0,2)
      CALL SYMBOL(0.5,5.0,.14,TITLE,0.0,LEN)
      CALL PLOT(0.,AY+DELY,-3)
      RETURN
      ENTRY PLOTFIN
      CALL PLOT(AX+2.,0.,999)
      RETURN
      END
```

SYMBOLIC REFERENCE MAP (R=2)

ENTRY POINTS		DEF LINE	REFERENCES
3	COMPLT	1	33
71	PLOTFIN	34	36

VARIABLES	SN	TYPE	RELOCATION								
212	AX	REAL		REFS	17	27	35	DEFINED	5		
213	AY	REAL		REFS	16	22	23	32	DEFINED	5	
214	DELY	REAL		REFS	16	32	DEFINED	5			
237	IB	INTEGER	ARRAY	REFS	3	8					
210	JOY	INTEGER		REFS	6	7	DEFINED	4	6		
0	LEN	INTEGER	F.P.	REFS	31	DEFINED	1				
0	M	INTEGER	PTS	REFS	2	22	2*23	2*27	38		
211	NGPH	INTEGER		REFS	14	15	16	DEFINED	4	14	18

SUBROUTINE COMPLT 73/74 OPT=1 FTN 4.6+433 07/30/82 10.33.24 PAGE 2

VARIABLES	SN	TYPE	RELOCATION						
0	TITLE	REAL	F.P.	REFS	31	DEFINED	1		
1	X	REAL	ARRAY PTS	REFS	2	2*27	38		
0	XTITLE	REAL	F.P.	REFS	27	DEFINED	1		
1001	Y	REAL	ARRAY PTS	REFS	2	22	2*23	38	
236	YP	REAL		REFS	17	DEFINED	16		
0	YTITLE	REAL	F.P.	REFS	23	DEFINED	1		

EXTERNALS	TYPE	ARGS	REFERENCES				
AXIS		8	23	27			
CCIDNT		3	10				
FACTOR		1	9	11			
LINE		6	38				
PLOT		3	12	17	32	35	
PLOTS		3	8				
SCALE		4	22				
SYMBOL		6	31				

STATEMENT LABELS		DEF LINE	REFERENCES
23	1	13	7
37	5	19	15

COMMON BLOCKS	LENGTH
PTS	1025

STATISTICS		
PROGRAM LENGTH	22118	1161
CM LABELED COMMON LENGTH	20018	1025

```
      PROGRAM LOOK(INPUT,OUTPUT)
      COMMON /PTS/ M,XX( 512),YY( 512)
      DIMENSION YY1( 512)
      DIMENSION YY2( 512),YY3( 512)
      DIMENSION FMT(5)
      DIMENSION RADIUS(4),PHIS(4),FREQS(4)
      DIMENSION BSS(3),BDD(3)
      COMPLEX PSI,BULK,SQUAT
      REAL KAY
      DATA RADIUS/2.E-4,2.E-4,20.E-4,20.E-4/
      DATA PHIS/.05,.10,.05,.10/
      DATA FREQS/100.E6,100.E6,50.E6,50.E6/
      DATA BSS/.05,.05,.05/
      DATA BDD/.01,.02,.05/
C
C
C
      PI=3.1415926536
      RHO1=1.13
      RHO2=.0012
      P1CD12=2.215E10
      P1CS12=.01E10
      P2CD22=1.42E6
      P2CS22=0.0
      CD1=1.40E5
C
      Q1=P1CD12/P2CD22
      Q2=(4.0/3.0)*P1CS12/P2CD22
      Q3=(4./3.)*P1CS12/P1CD12
      PTS=300.
      PTS=500.
      MAX=PTS
      LBSTA=1
      LBEND=3
      DO 2000 LBS=LBSTA,LBEND
      BS1=BSS(LBS)
      BD1=BDD(LBS)
      BD12=4.*BD1*BD1
      ENCODE(18,215,FMT)      BS1,BD1
  215 FORMAT(                                  * BS1=*,F4.2,*,BD1=*,
     1    F4.2)
      PRINT 215,      BS1,BD1
      PHIMAX=0.5
      DELTA=PHIMAX/PTS
      PHI=DELTA
      M=0
      DO 50 I=1,MAX
      M=M+1
C
C     BEGIN EQUATIONS
C
      AM=((6.*P1CD12 - 4.*P1CS12) + ((BS1+BS1)*
     1    (-16.*P1CD12*BD1 + 8.*P1CS12*BS1))) * (1.-PHI)
      BM=(-16.*P1CD12*BD1 + 8.*P1CS12*BS1 -
     1    ((BS1+BS1)*(8.*P1CD12 - 4.*P1CS12))) * (1.-PHI)
      KAY=6.*P1CD12 - 4.*P1CS12 + ((6.*P1CD12 + 4.*P1CS12)*PHI)
      CM=-16.*P1CD12*BD1 + 8.*P1CS12*BD1
```

```
     1    -((BS1+BS1)*(4.*P1CD12 - 4.*P1CS12)*PHI)
          BULK=CMPLX(EM,EN)/CMPLX(KAY,ELL)
60        YY(M)=REAL(BULK)
          YY1(M)=AIMAG(BULK)
          RX=REAL(BULK)
          RY=AIMAG(BULK)
          R1=SQRT(RX**2 + RY**2)
65        RCX=SQRT(0.5*(R1+RX))
          RCY=(RY/ABS(RY))*SQRT(0.5*(R1-RX))
          SQUAT=CMPLX(RCX,RCY)
          SQUAT=SQRT(.01E10/(RHO1*(1.-((1.-RHO2/RHO1)*PHI))))*SQUAT
          YY2(M)=REAL(SQUAT)
70        YY3(M)=AIMAG(SQUAT)
          XX(M)=PHI
          PHI=PHI+DELTA
     50   CONTINUE
          XX(M+1)=0.0
75        XX(M+2)=PHIMAX/5.
          PRINT 20,(XX(J),YY(J),J=1,M)
     20   FORMAT( 5(*  X=*, F7.5,*,Y=*,E10.4))
          CALL COMPLT( 10H   PHI    ,10HRE(EF.SHR) ,FMT,18)
          DO 400 J=1,M
80        YY(J)=YY1(J)
     400  CONTINUE
          PRINT 20,(XX(J),YY(J),J=1,M)
          CALL COMPLT( 10H   PHI    ,10HIM(EF.SHR) ,FMT,18)
          DO 500 J=1,M
85        YY(J)=YY2(J)
     500  CONTINUE
          PRINT 20,(XX(J),YY(J),J=1,M)
          CALL COMPLT( 10H   PHI    ,10HRE(CS2BAR) ,FMT,18)
          DO 600 J=1,M
90        YY(J)=YY3(J)
     600  CONTINUE
          PRINT 20,(XX(J),YY(J),J=1,M)
          CALL COMPLT( 10H   PHI    ,10HIM(CS2BAR) ,FMT,18)
     1000 CONTINUE
95   2000 CONTINUE
          CALL PLOTFIN
          END
```

SYMBOLIC REFERENCE MAP (R=2)

ENTRY POINTS		DEF LINE	REFERENCES
4112	LOOK	1	

VARIABLES		SN	TYPE	RELOCATION						
7606	BDD		REAL	ARRAY	REFS	7	37	DEFINED	14	
4543	BD1		REAL		REFS	2*38	39	42	52	54 57
					DEFINED	37				
4544	BD124	*	REAL		DEFINED	38				
7603	BSS		REAL	ARRAY	REFS	7	36	DEFINED	13	
4542	BS1		REAL		REFS	39	42	3*52	3*54	3*57

SUBROUTINE COMPLT 73/74 OPT=1 FTN 4.6+433 07/28/82 16.04.47

VARIABLES		SN	TYPE	RELOCATION						
0	TITLE		REAL	F.P.	REFS	31	DEFINED	1		
1	X		REAL	ARRAY PTS	REFS	2	2*27	30		
0	XTITLE		REAL	F.P.	REFS	27	DEFINED	1		
1801	Y		REAL	ARRAY PTS	REFS	2	22	2*23	30	
236	YP		REAL		REFS	17	DEFINED	16		
0	YTITLE		REAL	F.P.	REFS	23	DEFINED	1		

EXTERNALS	TYPE	ARGS	REFERENCES				
AXIS		8	23	27			
CCIONT		3	10				
FACTOR		1	9	11			
LINE		6	30				
PLOT		3	12	17	32	35	
PLOTS		3	8				
SCALE		4	22				
SYMBOL		6	31				

PAGE 2

STATEMENT LABELS		DEF LINE	REFERENCES
23	1	13	7
37	5	19	15

COMMON BLOCKS	LENGTH
PTS	1025

STATISTICS

PROGRAM LENGTH	22118	1161
CM LABELED COMMON LENGTH	20018	1025

DISTRIBUTION

	Copies
Chief of Naval Material	
Attn: MAT-03	1
Department of the Navy	
Washington, DC 20360	
Commander	
Naval Sea Systems Command	
Attn: SEA-063R1 (Daniel Porter)	1
SEA-063R (Dale Houser)	1
SEA-06 (Dr. D. J. Pastine	1
SEA-63D (Paul Sisler)	1
SEA-63X (CAPT P. Sullivan)	1
SEA-05H (Stephen Blazek)	1
PMS-406B (Dr. E. Liszka)	1
SEA-063Z (J. Palinkas)	1
Department of the Navy	
Washington, DC 20362	
Commander	
Naval Coastal Systems Center	
Attn: Dr. Donald Folds	1
Lyles Adair	1
Dr. John Wynn	1
Panama City, FLA 32407	
Commander	
David W. Taylor Naval Ship Research & Development Center	
Attn: Code 1900 (Dr. Maurice Sevik)	1
Dr. David Feit	1
Code 1965 (Dr. M. Rummerman)	1
Carderock, MD 20084	
Commander	
David W. Taylor Naval Ship Research & Development Center	
Attn: J. Eynck	1
Dr. J. Dickey	1
Annapolis, MD 21402	

	Copies
Commander	
Office of Naval Research	
Attn: Code 432 (Dr. A. Wood)	1
Code 420 (Dr. D. Bradley)	1
Code 410 (Dr. W. Condell)	1
Code 430 (Dr. A. Dyness)	1
Code 411MA (Dr. C. Holland)	1
Code 280 (A. Allinthorpe)	1
Arlington, VA 22217	
Commander	
Naval Ocean Systems Center	
Department of the Navy	
Attn: J. Campbell	1
H. Porter	1
S. Spiedell	1
San Diego, CA 92152	
Commander	
Naval Research Laboratory	
Attn: Dr. Sam Hanish	1
Dr. Louis Dragonette	1
Washington, DC 20375	
Commander	
Naval Underwater Systems Center	
Attn: Dr. R. Radlinsky	1
B. Myers (3631)	1
New London, CT 06321	
Naval Postgraduate School	
Department of the Navy	
Attn: Prof. H. Medwin	1
Technical Library (0212)	1
Monterey, CA 93940	
Superintendent	
U. S. Naval Academy	
Attn: Prof. D. Brill	1
Technical Library	1
Annapolis, MD 21402	

Commander
Naval Air Systems Command
Attn: Gerhard Heike 1
Paul Queen 1
Washington, DC 20361

Director
Defense Advanced Research Projects Agency
Attn: Dr. E. Whitman 1
(Naval Warfare Division)
Dr. Fred Patten (Rm. 721) 1
1400 Wilson Boulevard
Arlington, VA 22209

Applied Research Laboratory
Pennsylvania State University
Attn: S. Hayek
P. O. Box 30
State College, PA 16801

Director
Office of the Defense Director for
Research and Engineering 1
The Pentagon, Rm 3E114
Washington, DC 20801

Director
Los Alamos Scientific Laboratory
Theoretical Division
Attn: Dr. W. M. Visscher 1
P. O. Box 1663
Los Alamos, N M 87545

Chief Scientist
Cambridge Acoustical Associates
Attn: Dr. M. Junger 1
54 Rindge Avenue Extension
Cambridge, MA 02140

Weidlinger Associates
Attn: Dr. M. L. Baron 1
110 E. 59th Street
New York, N Y 10022

Director
Office of Naval Technology 1
800 N. Quincy Street
Arlington, VA 20360

Commanding Officer
Naval Ocean Research and Development
Activity
Attn: Dr. W. Kupperman 1
Bay St. Louis, MS 39529

Internal distribution:

R30	1
R40	1
R04	1
R43 (C. W. Lufcy)	1
R43 (Dr. G. Gaunaurd)	10
U20 (T. Harris)	1
E431	9
E432	3
E35	1


DAT
FILM